FIBRE BRAGG GRATING VIBRATION SENSING SYSTEM

SHIRLEY DIONG CHEA FONG

FACULTY OF SCIENCE
UNIVERSITY OF MALAYA
KUALA LUMPUR

2014

FIBRE BRAGG GRATING VIBRATION SENSING SYSTEM

SHIRLEY DIONG CHEA FONG

RESEARCH REPORT SUBMITTED IN FULFILLMENT OF THE REQUIREMENTS FOR THE DEGREE OF MASTER OF SCIENCE (APPLIED PHYSICS)

DEPARTMENT OF PHYSICS
FACULTY OF SCIENCE
UNIVERSITY OF MALAYA
KUALA LUMPUR

2014

ABSTRACT

In the recent decades, optical fibre sensors have become more reputational due to the fact that they are small in size, robust, light weight, immune to electromagnetic field and able to multiplex. This research report presents a nonlinear output response of an acousto-optically modulated distributed Bragg reflector (DBR). DBR used in this project is fabricated from two fibre Bragg gratings (FBGs) with similar Bragg wavelength, high reflectivity and slightly different bandwidth and a 12cm erbium-doped optical fibre. This structure of DBR is able to provide good throughput power. When impinged with acoustic waves, DBR gave an astounding result over the frequency range of 130 kHz to 190 kHz and power density of the ultrasound signal. The distorted output signal observed in the experiment matches the theoretical calculations based on transfer matrix method perfectly. Also, it is discovered that the distorted output signal generates second harmonic components. At higher amplitudes, amplitude of generated second harmonic will supersede the fundamental frequency. This finding is important for understanding the acousto-optic behaviour of DBR.

Abstrak

Semenjak kebelakangan ini, sensor gentian optik telah menjadi lebih reputasi kerana saiznya yang kecil, tahan lasak, ringan, imun kepada medan elektromagnet dan mampu multipleks. Laporan penyelidikan ini membentangkan respons isyarat keluaran yang tidak linear daripada acousto-optik termodulat Bragg reflektor teragih (DBR). DBR yang digunakan dalam projek ini adalah rekaan dari dua parutan serat Bragg (FBG) yang mempunyai panjang gelombang Bragg yang lebih kurang sama, pemantulan tinggi dan jalur lebar yang hampir sama berserta dengan gentian optik berpanjang 12cm yang didopkan dengan erbium. Struktur DBR ini mampu memberikan kuasa pemprosesan yang baik. Apabila impinged dengan gelombang akustik, DBR memberi keputusan yang mengejutkan untuk frekuensi antara 130 kHz hingga 190 kHz dan ketumpatan kuasa isyarat ultrasound. Isyarat output terpiuh didapati dari eksperimen tersebut adalah sepadan dengan pengiraan secara teori berdasarkan pemindahan kaedah matriks.Selain itu, isyarat output yang terpiuh ini juga didapati akan menjana komponen harmonik kedua. Pada amplitud yang lebih tinggi, amplitud harmonik kedua yang terjana akan menggantikan frekuensi asas. Penemuan ini adalah penting untuk memahami tingkah laku acousto- optik DBR.

ACKNOWLEDGEMENTS

First of all, I would like to express my sincere gratitude to my supervisor, Dr. Lim Kok Sing. He has been a tremendous mentor to me. I thank him for giving me this great opportunity to work in this dynamic and cutting-edge research area. This project would not have been a success without his profound knowledge, broad vision and patience guidance. It is an honour of me to be able to work with him.

I would also like to thank the colleagues in team especially Mr. Lai Man Hong and Mr. Lim Wei Sin. Thank you for helping me improve the experiments and also for your valuable advices which inspire me a lot. I would also like to thank all my coursemates especially Rebecca, Anas, Anusha, Fafa who supported me to strive towards my goal.

A special thanks to my family. Words cannot express how grateful I am to my parents. Without them, I would not have be where I am now. I would also like to thank my daughter for her understanding and support. Last but not least, I would like to express my greatest appreciation to my beloved husband who was always there to support me.

Contents

List of Figures

Chapter 2

Chapter 3

Chapter 4

List of Table

Chapter 1

Introduction

1.1 Motivation of the Work

Fibre Bragg grating (FBG) is a periodic modulation of refractive index along the core of single-mode optical fibres. This periodic structure acts as a filter for lights traveling along the fibre with the reflecting lights being predetermined by the Bragg wavelength. The grating formation is photogenerated when the core of a photosensitive optical fibre is exposed to UV laser.

FBG makes excellent fibre optic sensors because the gratings are integrated into the light guiding core of the fibre and are wavelength encoded. Thus, many problems of amplitude or intensity variations that plague other types of sensors are eliminated in FBG-based sensor (Othonos, et al. 2006).

Ultrasonic waves are often emit from a structure when there are defects within the structure. Stringent safety measures in modern structural health monitoring systems prefer FBG-based laser sensors over conventional electrical sensors like a piezoelectric transducer (PZT). This is due to low heat resistance due to curie temperature of the PZT and the unique fibre optic nature of FBGs that make it capable of multiplexing and have immunity to electromagnetic interference and power fluctuation along the optical path. (Tsuda 2010) (D.C. Seo 2009)

In the rising of global technology demand for better vibration sensing system, fibre optic sensors are widely investigated by researchers. For example, many studies have been done one the fibre Bragg grating lasing schemes like (i)employing FBG linearly to a broadband laser source (Tsuda, 2011), (ii) using an FBG sensor as the ring cavity mirror together with an optical amplifier to create a fibre ring laser (Tsuda

2010), (iii) employing a narrowband tunable laser source with small linewidth to directly convert FBG spectral shift into optical intensity (Fomitchov, et al. 2003), (iv) development of acoustic emission sensors based on distributed feedback (DFB) fibre grating laser (C.C. Ye, et al. 2005) and (v) demonstration of behaviour of distributed Bragg reflector (DBR) under the influence of acoustic wave. (Zhang, et al. 2009) (Comanici, et al. 2012) (Guan, et al. 2005) (Zhang, et al. 2008) (Lyu, et al. 2013)

DBR is a structure constructed by combining two wavelength matched FBGs as a resonator and a gain medium like erbium doped fibre as the fibre cavity between them. Studies have shown that DBR shares similar characteristics as FBG, have narrow linewidth and high optical signal-to-noise ratio. Therefore, in this project, DBR structure is used in the construction of an acoustic sensing system. To evaluate the system, which consist of a DBR acoustically modulated by a PZT, both theoretical and experimental analysis are carried out. This setup makes a simpler and lower cost acoustic sensing system.

1.2 Objectives

The objectives of this project are as stated below:

1. To construct a fibre Bragg grating vibration sensor.
2. To investigate the characteristics and frequency response of the sensor.

1.3 Project Overview

This report is organized as follows:

1. Chapter 1: Provides the background and the motivation of the project on fibre optic vibration sensing system.
2. Chapter 2: Introduces the basic knowledge of optical fibre, fundamentals of fibre Bragg grating (FBG), fabrication process of FBG, influence of acoustic waves on FBG and the structure of distributed Bragg reflector.
3. Chapter 3: Discuss the experiment setup and the methodology of the experiment.
4. Chapter 4: Presents the result, analysis and discussion on the experiment.
5. Chapter 5: Conclusion drawing for the project and suggestion for future works.

Chapter 2

Theoretical Background

2.1 Optical Fibre

Optical fibre is a thin, transparent and flexible strand that acts like lights pipes. It consists of a core and cladding where the core and cladding are made of the same type of material namely silica glass (SiO_2) of high chemical purity. The core and cladding of an optical fibre do not share the same refractive index where the refractive index in the core is relatively higher than the refractive index in the cladding. The slight changes in refractive index are done by doping of silica with low concentrations of doping materials like germanium, boron, titanium and etc. (Kasap 2001)

Optical fibres are classified into single mode fibres and multimode fibres. As illustrated in Figure 2.1, in a single mode fibre there is only one mode of lights that is propagating while in a multimode fibre, there are many modes of lights travelling. This is due to the design of the fibres where the core size of a single mode fibre is only 8-10μm in diameter while the multimode fibres have diameters ranging from 50-100μm.

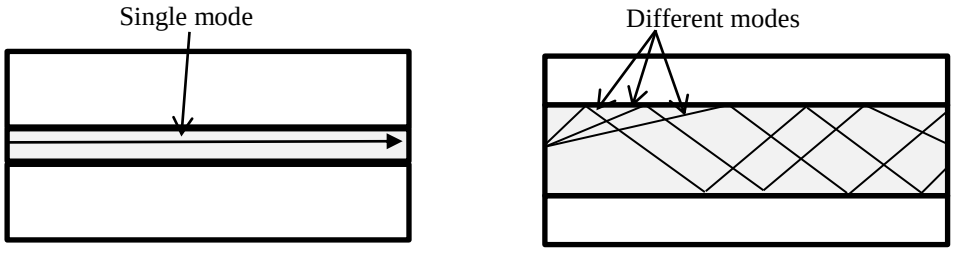

(a) Single mode fibre (b) Multimode fibre

Figure 2.1: Types of optical fibre

In conventional optical fibre design, the difference between refractive indices in the core and cladding are constant as depicted in Figure 2.2(a). This is called the step-index fibre design and this concept is widely used in single mode fibres and also step-index multimode fibres.

Designers have implemented graded-index design (as illustrated in Figure 2.2(b)) to overcome problems arises from many modes of lights propagating within the multimode fibres. Graded-index design has great impact on lights propagation and is able to overcome the differences among the group velocities of the modes that lead modal dispersion. In graded-index fibre, the refractive index is highest at the centre of the core fibre and gradually decreases to a minimum value at the core-cladding boundary. Hence velocities of the modes increase with the distance from the core axis since modes travelling farther away from core axis will travel a farther distance. All modes that propagate within the fibre will arrive at the end of fibre at the same time.

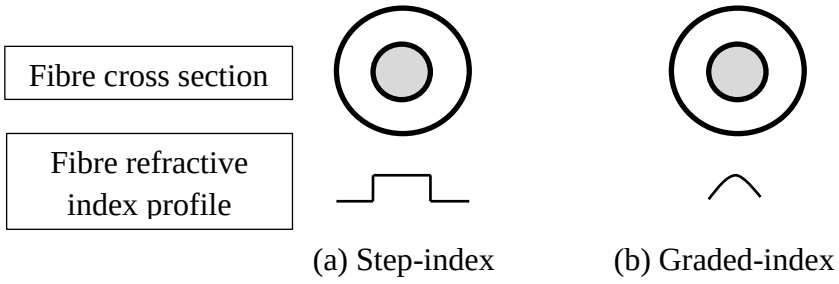

Figure 2.2: Refractive index profile of optical fibres

Although optical fibre is said to be the transporter for lights, not all source of radiation can be guided along an optical fibre. Only rays falling within a certain cone at the input can normally propagate through the fibre as illustrated in Figure 2.3.

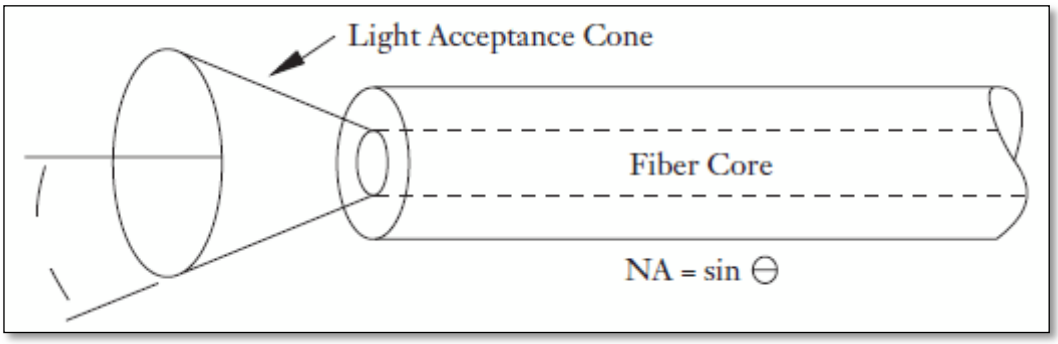

Figure 2.3: Light acceptance cone of fibre.

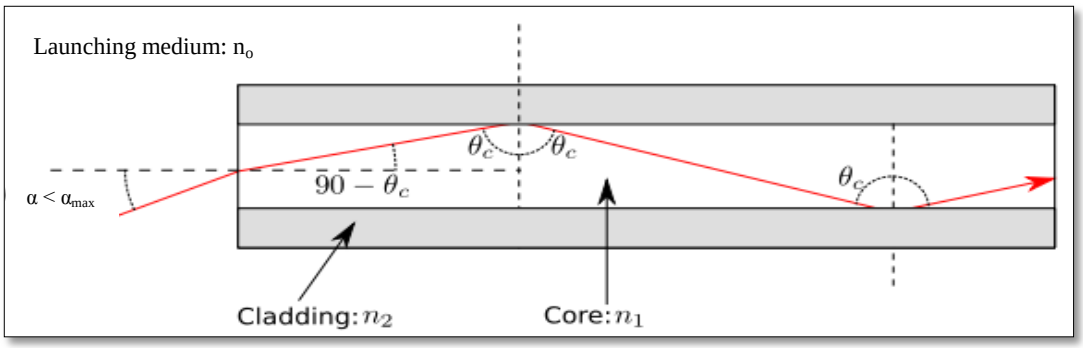

Figure 2.4: Maximum acceptance angle. (Othonos, et al. 2006)

Figure 2.4 shows the path of light ray launched from the outside medium of refractive index n_o into the optical fibre core. When light ray makes an angle θ with the normal of the fibre axis at the core-cladding interface, total internal reflection (TIR) will only occur if incident angle, θ is lesser than the critical angle θ_c, else the ray will escape into the cladding which will then escape out of fibre due to refractive index in cladding, n_2 is usually greater than refractive index of launching medium, n_0. Thus for light propagation within an optical fibre, the incident angle at the end of fibre core must be such that TIR is supported within the fibre.

From Snell's law, at the $n_o - n_1$ interface,

$$n_o \sin \alpha_{max} = n_1 \sin(90^o - \theta_c)$$

For TIR to occur at core-cladding interface,

$$n_1 sin\theta_c = n_2 \sin 90^o$$

$$sin\theta_c = \frac{n_2}{n_1}$$

Then, we can deduce that

$$\cos \theta_c = \frac{\sqrt{n_1^2 - n_2^2}}{n_1}$$

Hence,

$$\sin \alpha_{max} = \frac{n_1 \sin 90^o \cos \theta_c - \sin\theta_c \cos 90^o}{n_o}$$

$$\sin \alpha_{max} = \frac{n_1}{n_o} \frac{\sqrt{n_1^2 - n_2^2}}{n_1}$$

$$\sin \alpha_{max} = \frac{\sqrt{n_1^2 - n_2^2}}{n_0}$$

Numerical aperture, NA which is a characteristic parameter of optical fibre is the key factor in light launching designs into optical fibre. NA is defined in terms of refractive indices where

$$NA = \sqrt{n_1^2 - n_2^2}$$

So in terms of NA, maximum acceptance angle is defined as

$$\sin \alpha_{max} = \frac{NA}{n_0}$$

Therefore, total acceptance angle, $2\alpha_{max}$ is said to depend on the NA of the optical fibre and the refractive index of the launching medium.

2.2 Fundamentals of Fibre Bragg Gratings

2.2.1 Basic Bragg Grating

A fibre Bragg grating (FBG) is comprised of a periodic modulation of refractive index in the core of a single-mode optical fibre. These gratings create phase fronts that are perpendicular to the fibre's longitudinal axis as shown in Figure 2.5.

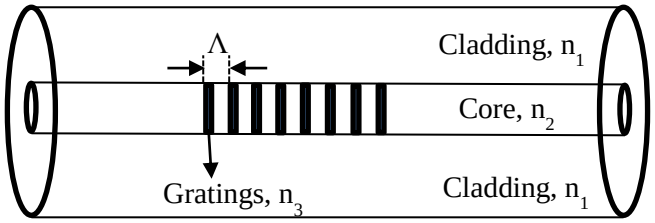

Figure 2.5: Illustration of fibre Bragg grating.

When lights are incident on the grating at angle θ_1, lights are diffracted and can be described by equation below

$$n \sin \theta_2 = \text{nsin}\, \theta_1 + m\frac{\lambda}{\Lambda}$$

where $\theta_2$is the angle of diffracted wave and m is the diffraction order as illustrated in Figure 2.6.

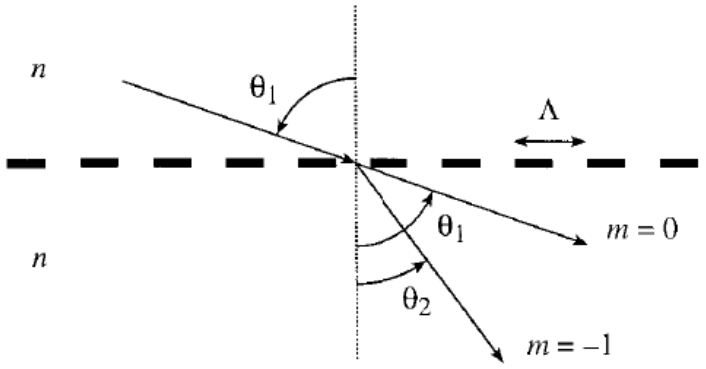

Figure 2.6: The diffraction of a light wave by a grating. (Saleh, et al. 1991)

Bragg grating requirements are to conserve both energy and momentum. In terms of conservation of energy, frequency of the incident radiation must be equivalent to the frequency of the reflected radiation ($hf_i = hf_f$). While in conservation of momentum, the wavevector of the incident wave, $\boldsymbol{\beta_1}$, plus the grating wavevector, $\boldsymbol{K} = \boldsymbol{m}\frac{2\pi}{\Lambda}$, must be equal to the wavevector of the scattered radiation, $\boldsymbol{\beta_2}$

$$\boldsymbol{\beta_1} + \boldsymbol{m}\frac{2\pi}{\Lambda} = \boldsymbol{\beta_2}$$

Since first-order diffraction usually dominates in a fibre grating, $\boldsymbol{m}$ = -1. Hence the momentum conservation condition becomes

$$2\left(\frac{2\pi n_{eff}}{\lambda_B}\right) = \frac{2\pi}{\Lambda}$$

$$\lambda_B = 2n_{eff}\Lambda$$

where λ_B is the Bragg grating wavelength that is the free space centre wavelength of the input light that will be reflected from the Bragg grating and n_{eff} is the effective refractive index of the fibre core at the free space centre wavelength.

2.2.2 Uniform Fibre Bragg Grating

Diffraction efficiency and spectral dependence of fibre gratings can be described using coupled-mode theory. The simplified coupled-mode equations for FBG written in a single mode fibre can be written as (Saleh, et al. 1991)

$$\frac{dR}{dz} = i\hat{\sigma}R(z) + i\kappa S(z)$$

$$\frac{dS}{dz} = -i\hat{\sigma}S(z) - i\kappa^{*}R(z)$$

where the amplitudes R and S are

$$R(z) \equiv A(z)e^{(i\delta z - \frac{\phi}{2})}$$

$$S(z) \equiv B(z)e^{(-i\delta z + \frac{\phi}{2})}$$

and a.c. coupling coefficient, κ, and d.c. self-coupling coefficient, $\hat{\sigma}$, are defined as

$$\kappa = \frac{\nu\pi\delta n}{\lambda}$$

$$\hat{\sigma} = \delta + \sigma - \frac{1}{2}\frac{d\phi}{dz}$$

The detuning δ, which is independent of z for all gratings, is defined to be

$$\delta = \beta - \frac{\pi}{\Lambda}$$

$$= \beta - \beta_D$$

$$= \frac{2\pi n_{eff}}{\lambda} - \frac{\pi}{\Lambda_o + \Delta\Lambda}$$

For single-mode Bragg reflection grating,

$$\sigma = \frac{2\pi}{\lambda}\overline{\delta n_{eff}}$$

$$\kappa = \kappa^* = \frac{\pi}{\lambda}v\overline{\delta n_{eff}}$$

If the grating is uniform along *z*, then δn_{eff} is a constant and possible chirp of grating, $\frac{d\phi}{dz} = 0$. Thus κ, σ and $\hat{\sigma}$ are constants.

The reflectivity of a uniform fibre grating of length *L* can be found by assuming a forward-going wave incident from $z = -\infty$ and requiring that no backward-going wave exists for $\geq \frac{L}{2}$. Hence, amplitude reflection coefficient, ρ and power reflection coefficient, *r* can be written as

$$\rho = \frac{-\kappa \sinh(\sqrt{\kappa^2 - \hat{\sigma}^2}L)}{\hat{\sigma}\sinh(\sqrt{\kappa^2 - \hat{\sigma}^2}L) + i\sqrt{\kappa^2 - \hat{\sigma}^2}\cosh(\sqrt{\kappa^2 - \hat{\sigma}^2}L)}$$

$$r = \frac{\sinh^2(\sqrt{\kappa^2 - \hat{\sigma}^2}L)}{\cosh^2\left(\sqrt{\kappa^2 - \hat{\sigma}^2}L\right) + \frac{\hat{\sigma}^2}{\kappa^2}}$$

Therefore, the maximum reflectivity r_{max} for Bragg grating is

$$r_{max} = \tanh^2(\kappa L)$$

and this occurs when $\hat{\sigma} = 0$, or at wavelength

$$\lambda_{max} = \left(1 + \frac{\overline{\delta n_{eff}}}{n_{eff}}\right)\lambda_D$$

where the design wavelength for Bragg scattering by infinitesimally weak grating with period Λ is given by $\lambda_D \equiv 2n_{eff}\Lambda$.

2.2.3 Coupled-mode and the T-matrix Formalism

T-Matrix formalism can be used to simulate the spectral characteristics of a Bragg grating structure. In this analysis, two counter-propagating plane waves are considered confined to the core of an optical fibre with a uniform Bragg grating length of *l* and uniform period of Λ as illustrated in Figure 2.7.

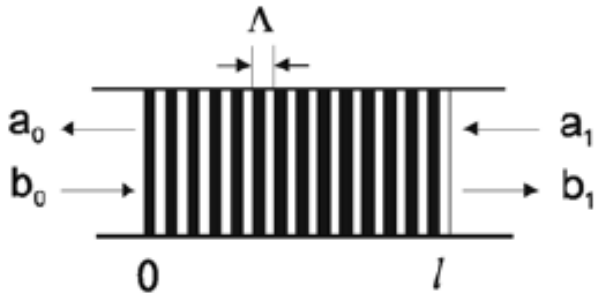

Figure 2.7: T-matrix model for single uniform Bragg grating (Erdogan 1997)

The electric fields of the backward-propagating and forward-propagating waves can be expressed as

$$E_a(x,t) = A(x)exp[i(wt - \beta x)]$$

$$E_b(x,t) = B(x)exp[i(wt + \beta x)]$$

where β is the wave propagation constant.

Assuming that there are both forward and backward inputs to the Bragg grating, and boundary conditions $B(0)=B_o$ and $A(l)=A_1$, closed-form solutions for A(x) and B(x) are obtained from equations

$$\frac{dA(x)}{dx} = i\kappa B(x)\exp[-i2(\Delta\beta)x]$$

$$\frac{dB(x)}{dx} = -i\kappa^* A(x)\exp[i2(\Delta\beta)x]$$

Following these assumptions,

$$a(x) = A(x)e^{(-i\beta x)}$$

$$b(x) = B(x)e^{(i\beta x)}$$

Therefore, the reflected wave, a_o, and transmitted wave, b_1, can be expressed by the scattering matrix

$$\begin{bmatrix} a_0 \\ b_1 \end{bmatrix} = \begin{bmatrix} S_{11} & S_{12} \\ S_{21} & S_{22} \end{bmatrix} . \begin{bmatrix} a_1 \\ b_0 \end{bmatrix}$$

with $a_1 = A_1 e^{(-i\beta l)}$, $b_0 = B_0$ and

$$S_{11} = S_{22} = \frac{i\sqrt{|\kappa|^2 - \Delta\beta^2}exp(-i\beta_0 l)}{-\Delta\beta \sinh\left(\sqrt{|\kappa|^2 - \Delta\beta^2}l\right) + i\sqrt{|\kappa|^2 - \Delta\beta^2}\cosh\left(\sqrt{|\kappa|^2 - \Delta\beta^2}l\right)}$$

$$S_{12} = S_{21} = e^{(2i\beta_0 l)} \frac{\kappa \sinh\left(\sqrt{|\kappa|^2 - \Delta\beta^2}l\right)}{-\Delta\beta \sinh\left(\sqrt{|\kappa|^2 - \Delta\beta^2}l\right) + i\sqrt{|\kappa|^2 - \Delta\beta^2}\cosh\left(\sqrt{|\kappa|^2 - \Delta\beta^2}l\right)}$$

Based on the scattering-matrix, the T-matrix for the Bragg grating is

$$\begin{bmatrix} a_0 \\ b_0 \end{bmatrix} = \begin{bmatrix} T_{11} & T_{12} \\ T_{21} & T_{22} \end{bmatrix} \cdot \begin{bmatrix} a_1 \\ b_1 \end{bmatrix}$$

where

$$T_{11} = T_{22}^{*} = e^{(-i\beta_0 l)} \frac{\Delta\beta \sinh\left(\sqrt{|\kappa|^2 - \Delta\beta^2}\, l\right) + i\sqrt{|\kappa|^2 - \Delta\beta^2} \cosh\left(\sqrt{|\kappa|^2 - \Delta\beta^2}\, l\right)}{i\sqrt{|\kappa|^2 - \Delta\beta^2}}$$

$$T_{12} = T_{21}^{*} = e^{(-i\beta_0 l)} \frac{\kappa \sinh\left(\sqrt{|\kappa|^2 - \Delta\beta^2}\, l\right)}{i\sqrt{|\kappa|^2 - \Delta\beta^2}}$$

Using T-matrix formalism, the reflection spectral response for uniform Bragg gratings can be calculated. In the calculations, it is assumed that the index of refraction change is uniform over the grating length. Theoretically, bandwidth of the gratings decreases with increasing length of grating. However, short lengths of grating are not easy to fabricate and error associated with the spacing between periods of a grating is cumulative. Therefore, with increasing grating length, the total error increases resulting in out-of-phase periods and broadening of Bragg grating spectrum.

2.2.4 Types of Bragg Grating

Different types of Bragg grating can be obtained by changing the inscription condition, type of laser used and the photosensitivity of the fibre as well as the type of optical fibre prior to the inscription process. Generally there are four types of fibre Bragg gratings where gratings formed at low intensities are generally said to be Type I while Type II are formed when energy of writing beam is higher.

Type I Fibre Bragg Grating

This type of grating has its reflection spectra of guided mode being the complementary of its transmission spectra. This implies that the loss due to absorption or reflection into the cladding is negligible. On top of that, Type I gratings can be erased at temperature of about 200^{o}C.

Type IA Fibre Bragg Grating

Type IA gratings may be considered the subtype of Type I gratings because they also have the transmission and reflection spectra that are complementary to each other. They are formed after prolonged UV exposure of a standard grating in hydrogenated germanium-doped fibre. Type IA gratings are unique because during inscription, large red shift is seen in the Bragg wavelength. On top of that, this type of gratings exhibits the lowest temperature coefficient.

Type II Fibre Bragg Grating

Type II gratings formed when physical damage is caused in the fibre core during the writing process and it produces very large refractive-index modulations. The gratings generally tend to have an irregular reflection spectrum due to ‘hot spots’ in the laser beam profile. Type II gratings pass wavelengths longer than the Bragg wavelength, whereas shorter wavelengths are strongly coupled into the cladding. In terms of stability, this type of gratings shows great stability at high temperatures hence it can be utilized for sensing applications in hostile environments.

Type IIA Fibre Bragg Grating

This type of grating is formed in non-hydrogen-loaded fibres at low power densities or with pulsed laser after long exposure. Although it also has transmission and reflection spectra that are complementary, Type IIA can be distinguished under dynamic conditions either in the initial fabrication or in the temperature erasure of the gratings. A clear advantage of Type IIA gratings over the Type I is the dramatically improved temperature stability of the grating which enables it to be used in high ambient temperatures.

2.3 Fabrication of Fibre Bragg Gratings

When ultraviolet light radiates an optical fibre, the refractive index of the fibre is changed. This photosensitivity phenomenon enables gratings to be written permanently on the optical fibre when the photo-exposed optical fibre is annealed appropriately for a few hours at temperatures above its maximum operating temperatures. The magnitude of the refractive index change (Δn) depends on factors like irradiation conditions (wavelength, intensity and total dosage of irradiating light), the composition of the core material and the any processing on the optical fibre prior to the irradiation for example "hydrogen loading" or "flame brushing". (Hill, et al. 1997)

The first inscription on optical fibre was demonstrated by Hill and co-workers in 1978 using a simple experimental set-up as shown in Figure 2.8. In the set-up, a blue Argon laser with wavelength of 488nm was used as the source where the incident laser light will interfere with the reflection forming standing wave pattern within the core of the fibre. At high intensity point, the refractive index will be changed permanently. Although the set-up is simple, this method is not preferred for the gratings will only function at wavelength near to the wavelength of the writing light.

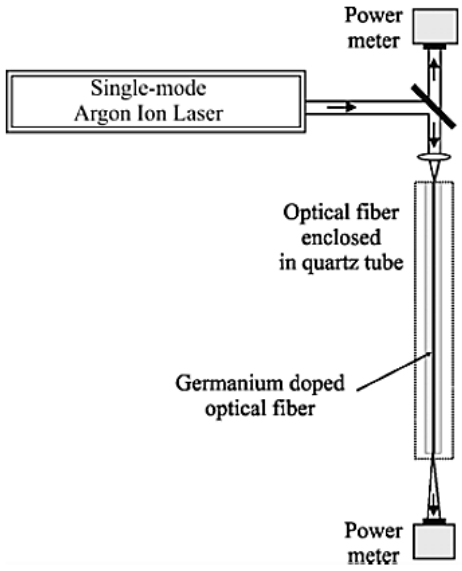

Figure 2.8: A typical apparatus used for recording Bragg gratings. (Erdogan 1997)

Due to the potential of FBG's applications, many methods have been explored like two-beam interferometric fabrication technique (Zhou, et al. 2003), phase-mask technique (Yu, et al. 2002) and point-by-point fabrication (Malo, et al. 1993).

Two-beam interferometric technique was first explored by Meltz and his co-workers in 1989 and his method is the holographic method. Their setup is shown in Figure 2.9. In this fabrication method, a tuneable excimer-pumped dye laser operating at wavelength range of 486-500nm is used to provide UV laser source of 244nm. The transmission spectrum of FBG is monitored in real time and by varying the period of refractive index modulation, Λ, an FBG can be obtained.

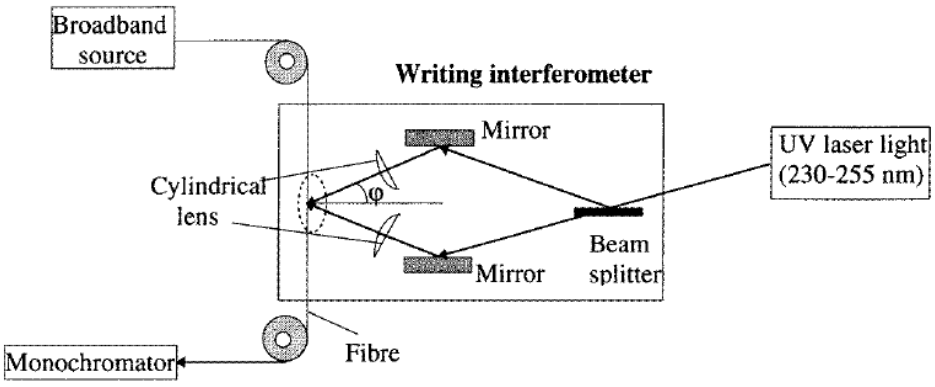

Figure 2.9: Schematic diagram of the two-beam interferometer method. (Rao 1997)

The advantage of interferometric fabrication is that it is easy to adjust the angle between the two beams to create different periods as illustrated in Fig. 2.10. This will ease fabrication of FBG with different wavelengths. So, many researchers have studied and improve on this method. Kashyap *et al* 1990 did modifications based on wavefront splitting rather than amplitide splitting as in holographic method. Askins *et al* 1992 demonstrated ultrafast fabrication of FBG with a single 20ns pulse laser. However,

two-beam interferometer method requires stable set-up and a highly coherence light source that is very expensive.

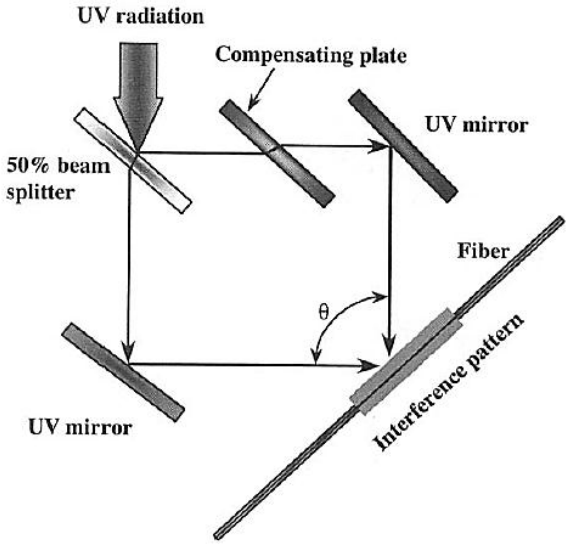

Figure 2.10: UV interferometer for writing Bragg gratings in optical fibre. (Erdogan 1997)

Another method to fabricate FBG is the phase-mask technique. This method was discovered by Hill *et al* in 1993. A phase-mask is diffractive element that can be used to form an interference pattern laterally. FBG fabrication using a phase-mask method utilizes a phase-mask to spatially modulate the UV writing beam as illustrated in Figure 2.11. When UV laser is incident on the phase-mask, an interference pattern between the first-plus order and first-minus order of the diffracted beams will imprint a refractive index modulation into the core of a photosensitive optical fibre as illustrated in Figure 2.12. UV laser sources used in this method have low spatial and temporal coherence, so the photosensitive optical fibre must be placed near but not in contact and parallel with the phase-mask to maximize the modulation of the refraction index and at the same time not damaging the phase-mask.

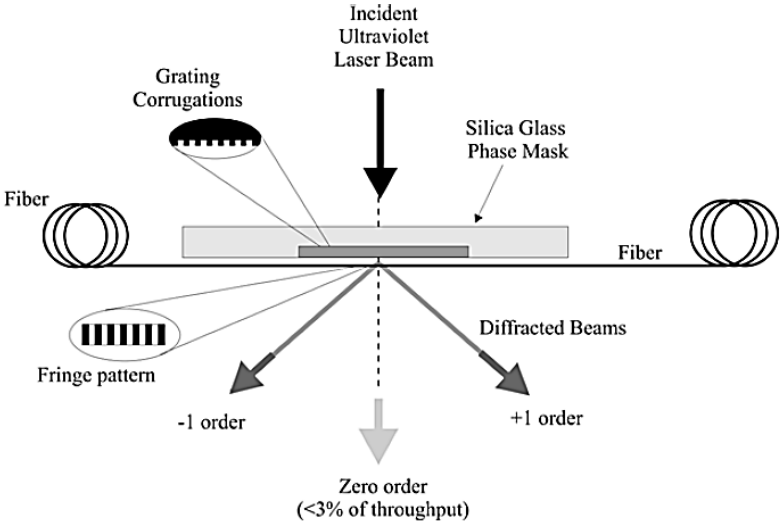

Figure 2.11: Phase-mask geometry for inscribing Bragg gratings in optical fibres.(Erdogan 1997)

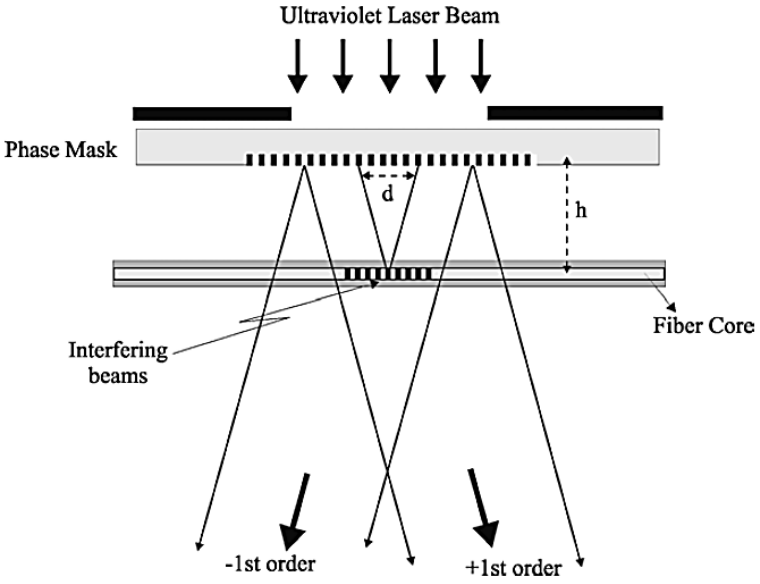

Figure 2.12: A schematic of the diffraction from the phase-mask. (Erdogan 1997)

The significant advantages of phase-mask technique are Bragg wavelength of the FBG is determined by the pitch of the phase-mask and independent to the wavelength of the UV laser source. Also the requirement for coherent UV laser source is reduced; hence cheaper UV laser source can be used in FBG fabrication. On top of that, the combination of single-beam writing method with the use of phase-mask that are produced from a digitally-controlled photolithography process improves the stability of FBG writing and makes it highly repeatability and low in cost for mass production.

Since there are many advantages in fabrication of FBG using this method, varies improvement methods have be studied and discovered. Prohaska *et al* 1993 used a diverging or converging wavefront incident on a fixed phase-mask to tune the Bragg wavelength of the FBG. Mask scanning method was studied by Martin and Ouellette 1994, Rourke *et al* 1994, Kashyap *et al* 1994 and this method managed to produce gratings with high reflectivity and low bandwith. In 1995, Cole *et al* demonstrated moving fibre/phase-mask method where fibre is moved relative to mask while the UV beam is scanning and he successfully fabricated FBGs with different wavelengths using only one phase-mask.

2.4 Influence of acoustic waves on FBG

When lights propagates through the fibre grating, its phase, ϕ can be described as

$$\phi = \beta L$$

where β is the propagation constant and L is the length of fibre.

When acoustic wave is exerted onto an optical fibre with diameter D, pressure change causes mechanical strain. Its induced phase shift can be written as (Hocker 1979)

$$\Delta\phi = L\Delta\beta + \beta\Delta L$$

with

$$L\Delta\beta = L\frac{d\beta}{dn}\Delta n + L\frac{d\beta}{dD}\Delta D$$

$$\beta\Delta L = \frac{\beta(1-2v)LP}{E}$$

where

- E is the Young's modulus of the fibre
- v is Poisson's ratio.
- $\beta\Delta L$ denotes the change in physical length of the fibre that changes the grating pitch
- $L\frac{d\beta}{dn}\Delta n$ shows the elasto-optic effect where the refractive index changes due to incident ultrasonic waves.
- $L\frac{d\beta}{dD}\Delta D$ denotes the waveguide mode dispersion effect due to the change in fibre diameter produced by the ultrasonic-induced strain.

Ultrasound impinging on an FBG can be detected by the FBG because it sensed a minute shift in Bragg wavelength as depicted in Figure 2.13. (Tsuda 2011) This phenomenon originated from the refractive index of the fibre and the FBG period being modulated as ultrasonic waves induce mechanical strain in the fibre through photo-elastic effect as shown in Figure 2.14. (Fomitchov, et al. 2003)

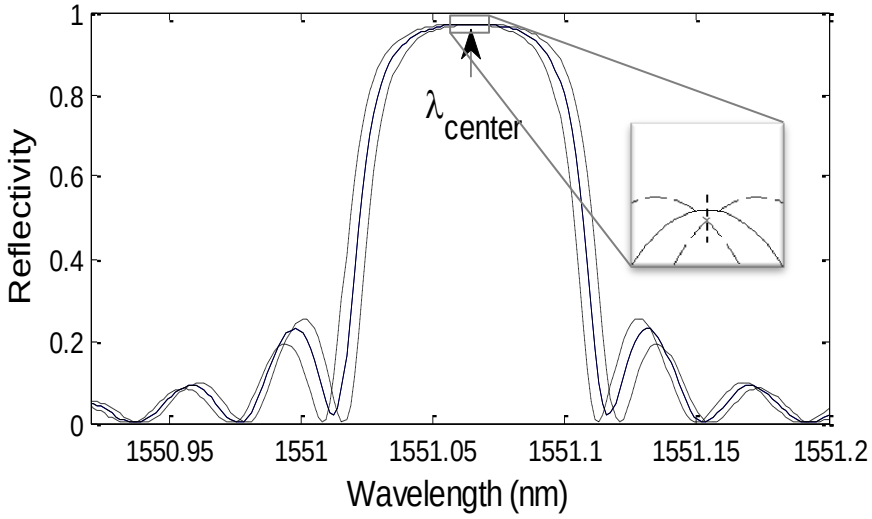

Figure 2.13: Simulated reflection spectra of a 2cm uniform FBG impinged with 150kHz flexural vibration. The dashed curves are the results of impinged acoustic wave with a phase difference of π and –π from that of solid curve.

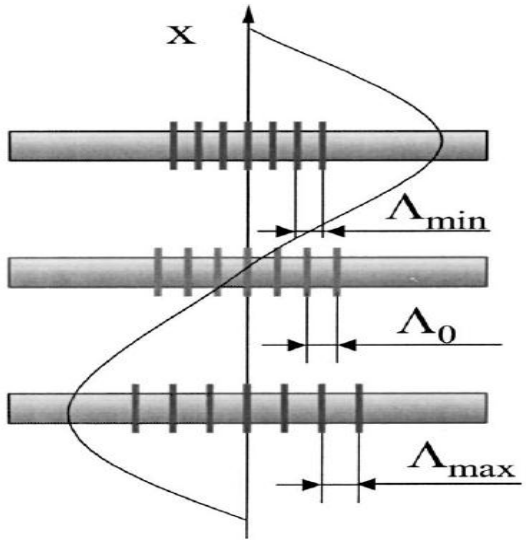

Figure 2.14: Modulation of the FBG period by acoustic pressure.(Fomitchov, et al. 2003)

FBG ultrasound detection system is classified according to the type of light source used. When a broadband light source is being employed, wherein an optical filter is used to demodulate the FBG sensor signal, the spectrum of the optical filter must overlap the reflective spectrum of the FBG sensor to detect ultrasound. The other type of light source for ultrasound detection involves a laser-demodulation system, where a laser is tuned to a wavelength where the slope of FBG reflective spectrum is steep like in a distributed Bragg reflector (DBR) and distributed feedback (DFB). (Guan, et al. 2012)

Considering a single mode fibre and plane ultrasonic wave at normal incidence, the changes in physical length L and refractive index n of the fibre can be written as a function of pressure ΔP. (Rao 1997)

$$\frac{\Delta L}{L} = \frac{-(1-2\upsilon)\Delta P}{E}$$

$$\Delta n = \frac{n^3 \Delta P}{2E}(1-2\upsilon)(2\rho_{12}+\rho_{11})$$

where E is the Young's modulus, υ is the Poisson's ratio, ΔP is the pressure variation caused by acoustic waves, ρ_{12} and ρ_{11} are the fibre strain tensor components.

Given that from Equation 2.7, for a pressure change of ΔP, the corresponding wavelength shift $\Delta\lambda_{BP}$ is given by

$$\frac{\Delta\lambda_{BP}}{\lambda_B} = \frac{\Delta(n\Lambda)}{n\Lambda} = \left(\frac{1}{\Lambda}\frac{\partial\Lambda}{\partial P} + \frac{1}{n}\frac{\partial n}{\partial P}\right)\Delta P$$

Since the change of grating period is the same as that of optical fibre length,

$$\frac{\Delta\Lambda}{\Lambda} = \frac{\Delta L}{L}$$

The normalized pitch-pressure and the index-pressure coefficients are given by

$$\frac{1}{\Lambda}\frac{\partial\Lambda}{\partial P} = \frac{-(1-2v)}{E}$$

$$\frac{1}{n}\frac{\partial n}{\partial P} = \frac{n^2\Delta P}{2E}(1-2v)(2\rho_{12}+\rho_{11})$$

Hence the wavelength-pressure sensitivity is given by

$$\Delta\lambda_{BP} = \lambda_B\left[\frac{-(1-2v)}{E} + \frac{n^2}{2E}(1-2v)(2\rho_{12}+\rho_{11})\right]\Delta P$$

From the equation, it is shown that the wavelength shift of the FBG is directly proportional to the pressure change in this case the acoustic pressure change, ΔP. The above equation is only valid for the case of normal incident of low-frequency acoustic waves with wavelengths significantly larger than the diameter of the optical fibre. For acoustic wavelength that is comparable with the diameter of the fibre, the acoustic pressure induces different index changes and therefore changes the physical length and grating periods.

2.5 Distributed Bragg Reflector (DBR) Fibre Laser Structure

DBR fibre laser is constructed from the combination of two wavelength-matched fibre Bragg gratings and a short segment of active fibre like co-doped Er/Yb fibre (Zhang, et al. 2009) (Comanici, et al. 2012) (Guan, et al. 2005) (Zhang, et al. 2008) and erbium-doped fibre (Lyu, et al. 2013). The FBGs function as mirrors to provide optical feedback and form a laser cavity as illustrated in Figure 2.15.

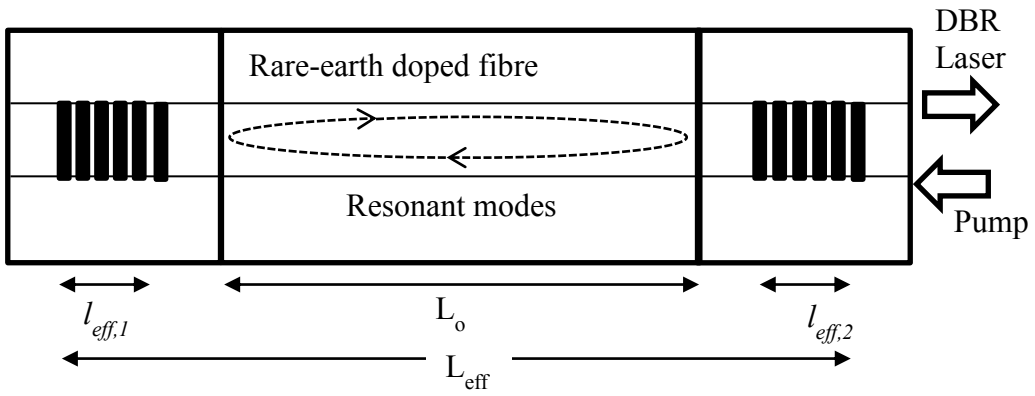

Figure 2.15: Schematic of DBR fibre laser sensor.

Referring to Figure 2.15, there will be many modes resonating within the cavity and the resonant wavelength can be expressed by

$$\lambda_{res} = \frac{2nL_{eff}}{M}$$

where n is the modal index, M is the order of the resonant mode and L_{eff} is the effective cavity length.

Most DBR fibre lasers have the resonant mode spacing much smaller than the grating reflection bandwidth. Therefore, there will be several modes lasing within the cavity, but only the dominant mode will oscillates and the others will be suppressed and normally lasers operate in a single-longitudinal mode. However, when DBR is subjected to external perturbations, mode hopping will occur and this limits the

practical applications of the DBR. To overcome this problem, the cavity length needs to be shortened. (Zhang, et al. 2009)

From Figure 2.15, the effective cavity length is defined as

$$L_{eff} = l_{eff,1} + L_o + l_{eff,2}$$

with L_o is the grating spacing, $l_{eff,1}$ and $l_{eff,2}$ are the effective lengths of the two Bragg gratings.

The effective lengths of FBGs are given by the dispersion properties of the FBGs,

$$l_{eff} = l_g \frac{\sqrt{R}}{2atanh(R)}$$

where l_g is the length of the grating and *R* is the reflectivity of the FBG.

Hence, higher reflectivity of FBGs as mirrors shortens the cavity which helps in ensuring only one longitudinal mode output. On top of that, FBGs with high reflectivity also help to prevent round-trip loss when oscillating within the laser cavity, therefore, larger laser emission also can be produced. Note that the competition between different longitudinal modes is much stronger than competition between two different polarization modes.

A DBR fibre laser naturally emits laser output with two orthogonal states of polarizations and this causes energy fluctuations when they compete. So, polarization beat signal is used to measure external perturbations. The beat frequency is given by

$$\Delta\nu = \nu_x - \nu_y = \frac{c}{n_o\lambda_o}B$$

where n_o is the average index of the fibre, λ_o is the Bragg wavelength of the fibre grating and B is the modal birefringence, $B = |n_x - n_y|$.

Chapter 3

Methodology

3.1 Fabrication of Fibre Bragg Grating

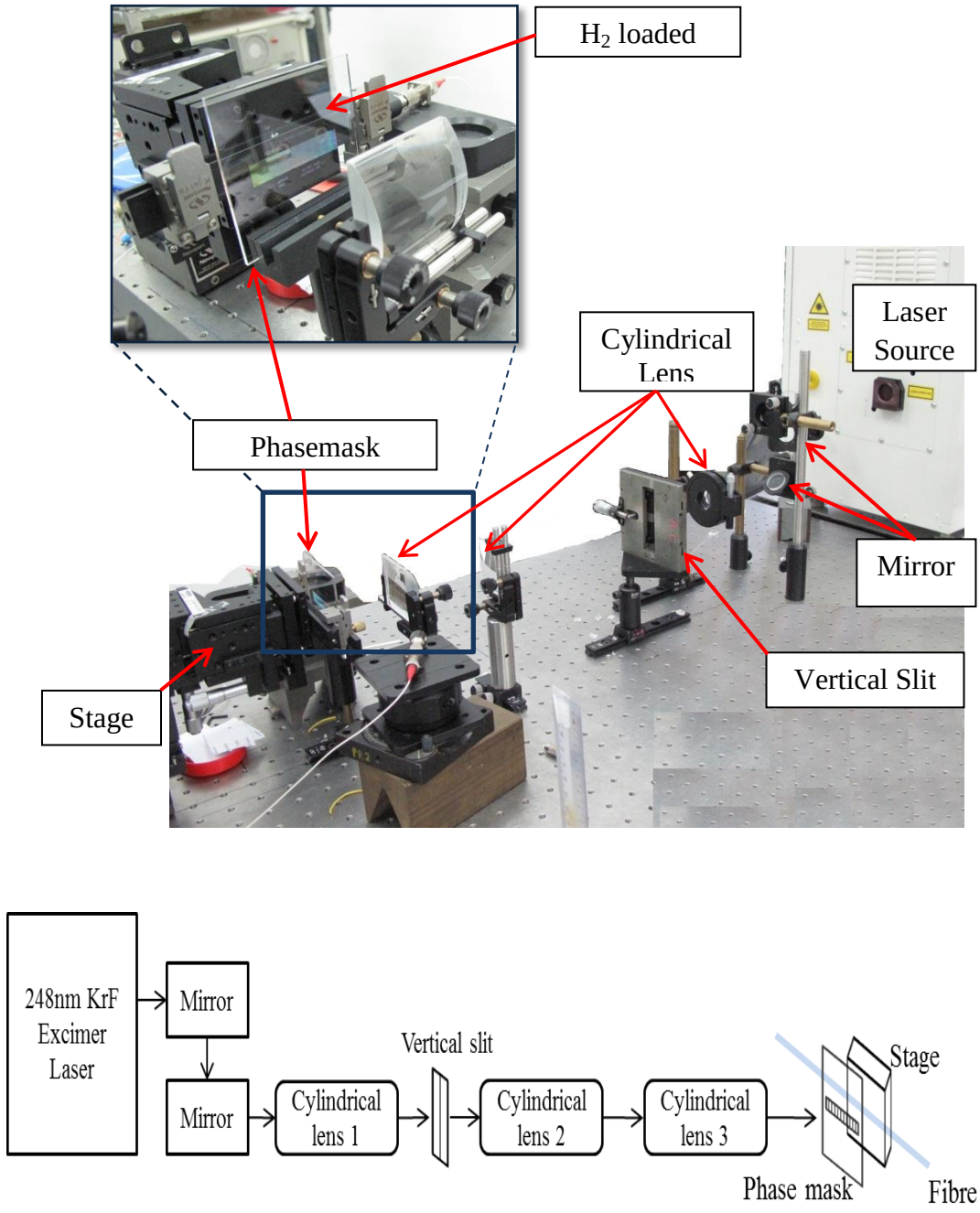

Figure 3. 1: Experimental setup and schematic diagram of FBG inscriptions.

The FBGs are fabricated using phase-mask grating-writing technique with a 248nm KrF excimer laser. Before the writing process, SMF-28 fibres are pre-soaked in a hydrogen tank at 1700psi for 7 days to enhance the photosensitivity of the optical fibres. On the 8^{th} day, grating inscription was performed using the mentioned excimer laser and phase-mask as shown in Figure 3.1.

The function of the mirrors is to lower the laser beam to setup height. Three cylindrical lenses are being used for beam shaping. The first two lenses with focal length of 25mm and 200mm respectively are used to expand the beam size from about 6mm to 45mm and they are placed at approximately 225mm apart. In between the first two lenses, a vertical slit is used to control the beam size of the laser beam by removing the tails of the Gaussian beam and obtaining uniform beam intensity. The third lens' function is to focus the beam before it strikes the phase-mask. According to the datasheet of the lens, the distance between the third lens and the target optical fibre must be approximately 67mm apart. Phase-mask at the end of the setup will create an interference pattern laterally on the target fibre which will then determines the grating structure of the FBG according to the refractive index modulation of the phase-mask. Real-time monitoring of FBG writing was done by observing the FBG transmission spectrum through an Optical Spectrum Analyser (OSA) during the UV laser writing process to ensure desired specification of grating reflectivity, wavelength and reflection bandwidth are achieved.

The fabricated FBGs are then annealed at $90^{o}C$ for 4 hours to accelerate the outwards diffusion of the residue hydrogen gas in the fibre and hence stabilize the properties of the FBGs like its reflectivity and also its Bragg wavelength.

3.2 Construction of Distributed Bragg Reflector Fibre Laser

A DBR was constructed by splicing two FBGs to both ends of an Erbium-doped fibre (EDF) which acts as a gain medium. In this experiment, a 12 cm long Metrogain EDF model DF1500L from Fibercore Ltd. with erbium ion concentration of 990ppm and absorption coefficients of 18.06dB/m at 1530nm was used. Figure 3.2 shows the schematic of the manufactured DBR. The FBGs used have negligible difference in wavelengths of about 0.001nm.The arrangement of FBGs is such that the reflectivity of FBG 2 which is nearer to the laser source is lower (35.8dB) than the reflectivity of FBG 1 (38.1dB) that is placed farther away from the laser source. This configuration will cause laser to oscillate between the two gratings and gain higher power within the gain medium hence creating higher output laser emission through the lower reflectivity FBG (FBG 2).

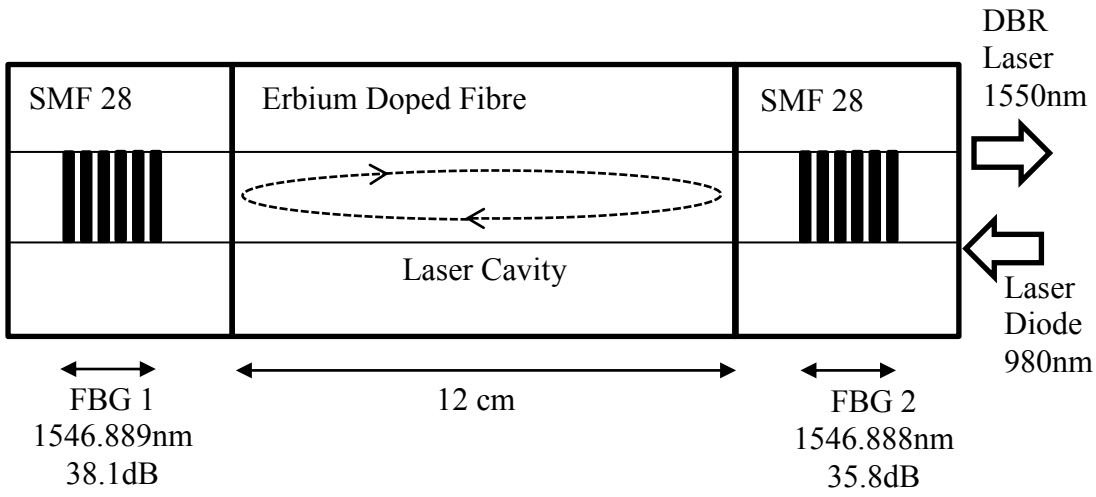

Figure 3.2: Schematic diagram of DBR fibre laser sensor.

3.3 Experimental Setup

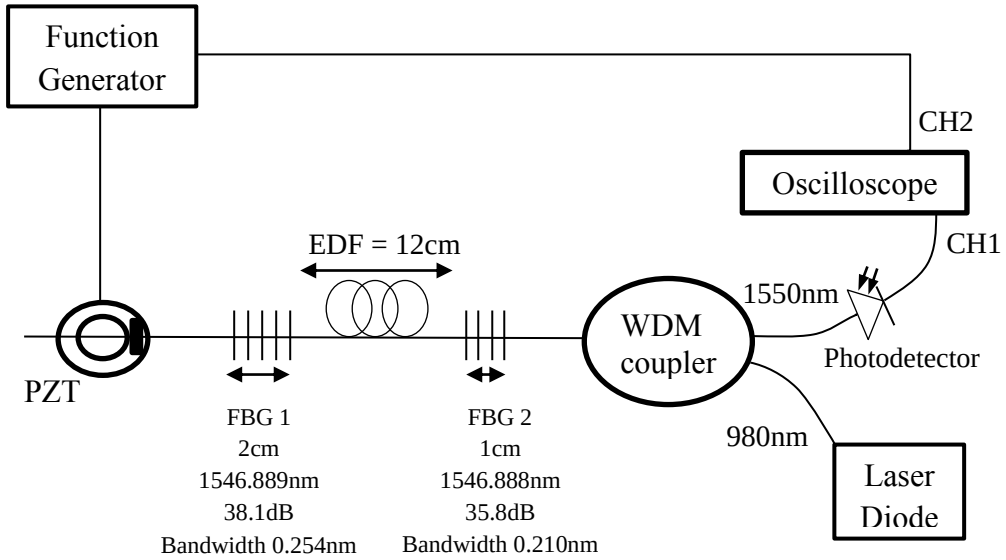

WDM - wavelength-division multiplexing
EDF - Erbium-doped fiber
PZT – Piezoelectric Transducer
CH1 – channel 1 of oscilloscope
CH2 – channel 2 of oscilloscope

Figure 3.3: Schematic diagram of experimental setup.

The DBR fibre laser was pumped by a 980nm laser diode through a wavelength-division multiplexing coupler as shown in Figure 3.3. Besides coupling pump laser source to DBR, WDM coupler also collects the throughput from the DBR to a photodetector. Photodetector will then convert the received optical signal to electrical signal before channelling it to an oscilloscope for recording and analysing purposes.

The first section of the experiment is to study the response of the DBR towards different pump power. This is done by changing the power of the laser diode and recording the response of DBR in channel 1 of the oscilloscope (CH1).

The next section of experiment involves investigation of the response of the DBR towards different acoustic pressure. This is done by connecting a piezoelectric transducer (PZT) at the free end of the DBR as shown in Figure 3.3. PZT is used to provide acoustic waves to the system when connected to a function generator. The throughput of the DBR due to acousto-optically modulated signals are recorded in channel 1 (CH1) of the oscilloscope while the acoustic waves of the PZT is recorded in channel 2 (CH2) of the oscilloscope.

In the last section of the experiment, the frequency response of the DBR was investigated for frequency ranging from 120 kHz to 190 kHz.

All acquired data collected from the oscilloscope is in time domain. To transform the data into frequency domain, fast fourier transformation was done using Matlab.

Chapter 4

Results, Analysis and Discussion of Experiment

4.1 Fabrication of Fibre Bragg Gratings

From the T-matrix formalism in Section 2.2.3, it is known that grating lengths does influence the quality of the gratings i.e. its reflectivity and bandwidth. Hence, before the FBG fabrication process, a simulation of effect of grating length was studied as attached in Appendix 1.

Table 4.1: Simulation parameters

n_{eff}	1.445
λ_D	1558nm
δn_{eff}	2×10^{-4}
L	0.05

The simulation is based on data in Table 4.1 and the results of the simulation are shown in Figure 4.1. It is found that with the increase of grating lengths, the reflectivity will increase while the bandwidth of the gratings will decrease. However, eventually the reflectivity will be saturated with lengthier gratings. Hence, in this project, the length of grating selected is less than 3cm.

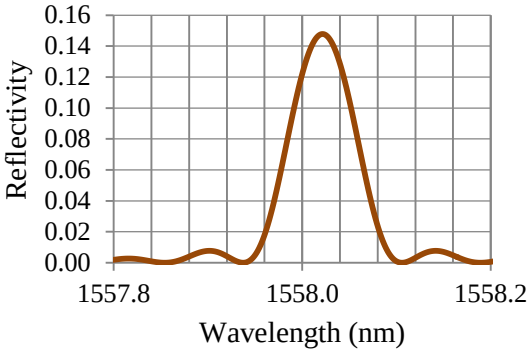

(a) Grating length = 0.01m

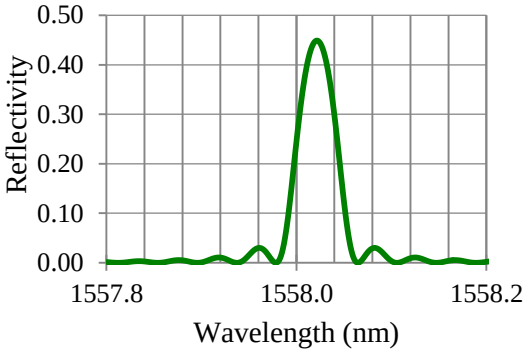

(b) Grating length = 0.02m

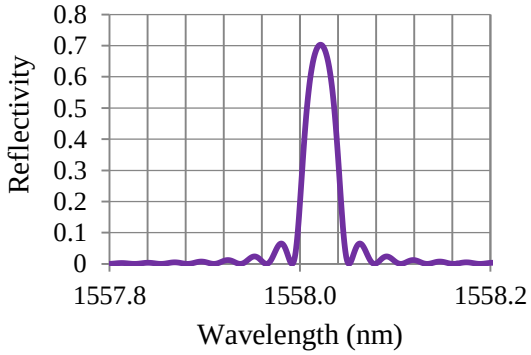

(c) Grating length = 0.03m

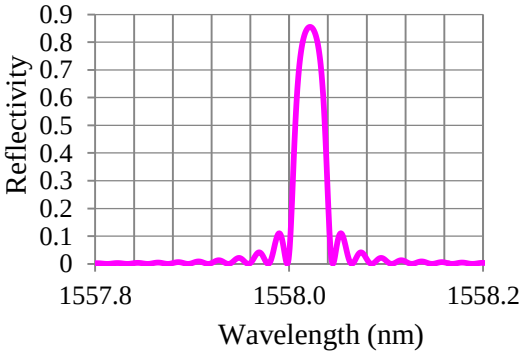

(d) Grating length = 0.04m

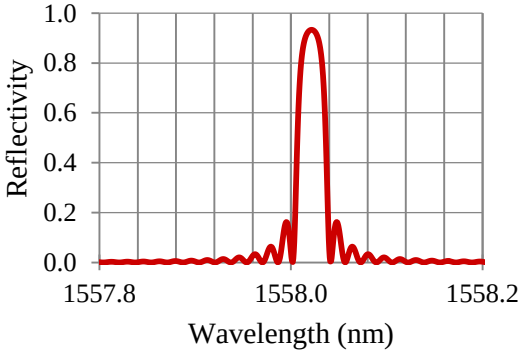

(e) Grating length = 0.05m

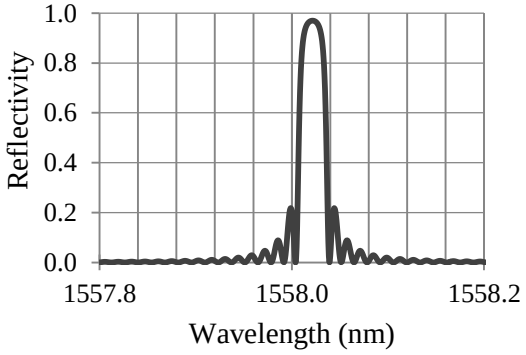

(f) Grating length = 0.06m

Figure 4. 1: Simulation for response of grating lengths.

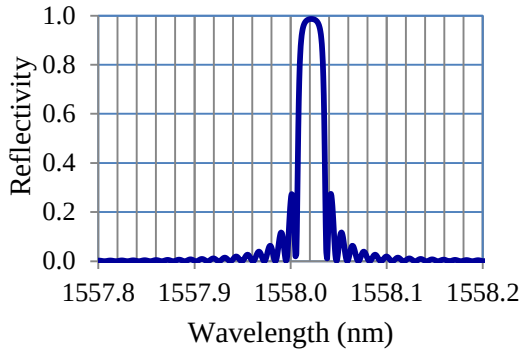

(g) Grating length = 0.07m

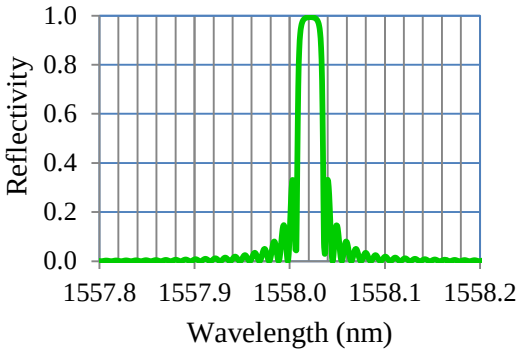

(h) Grating length = 0.08m

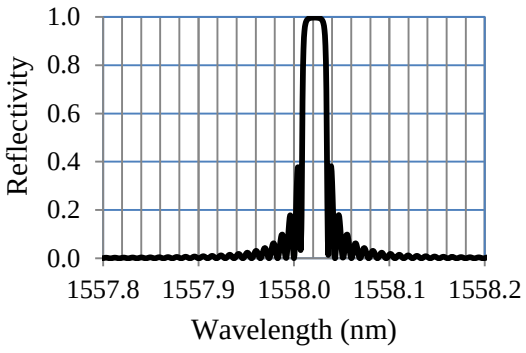

(i) Grating length = 0.09m

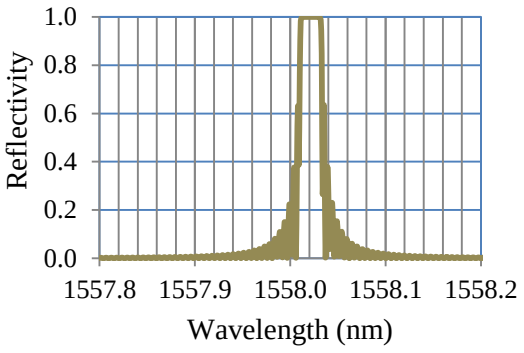

(j) Grating length = 0.15m

Figure 4.1, continued: Simulation for response of grating lengths.

As mentioned in Section 3.1, after the FBG writing process, characteristics of FBG can be observed through an Optical Spectrum Analyser, OSA. Figure 4.2 shows the reflection spectrum of fabricated FBGs. By observing the spectrum, the Bragg wavelength, bandwidth and grating reflectivity can be obtained. Say for example, in Figure 4.2 (a), the bandwidth of the FBG is 0.21 nm while the Bragg wavelength 1547.1 nm. Figure 4.2(b) on the other shows FBG with a Bragg wavelength of 1547.6nm and bandwidth of 0.20nm. These two FBGs are matched in terms of Bragg wavelength and hence are can be used to construct a DBR. Many FBGs were fabricated and the best matched FBGs are used to construct a DBR.

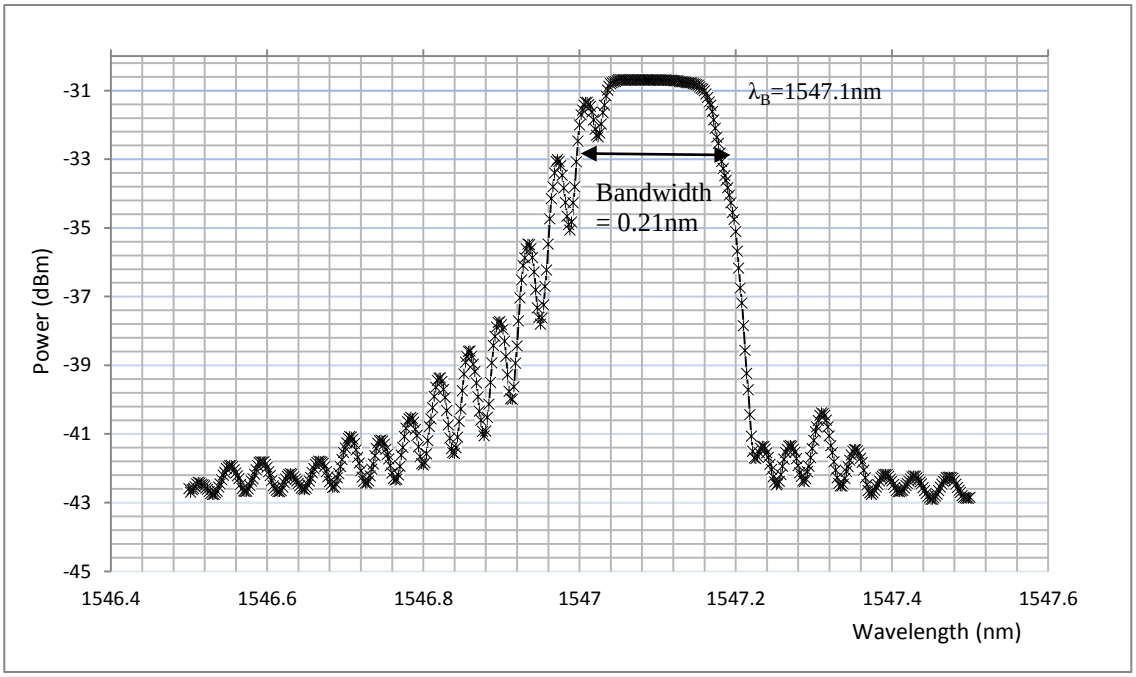

(a)

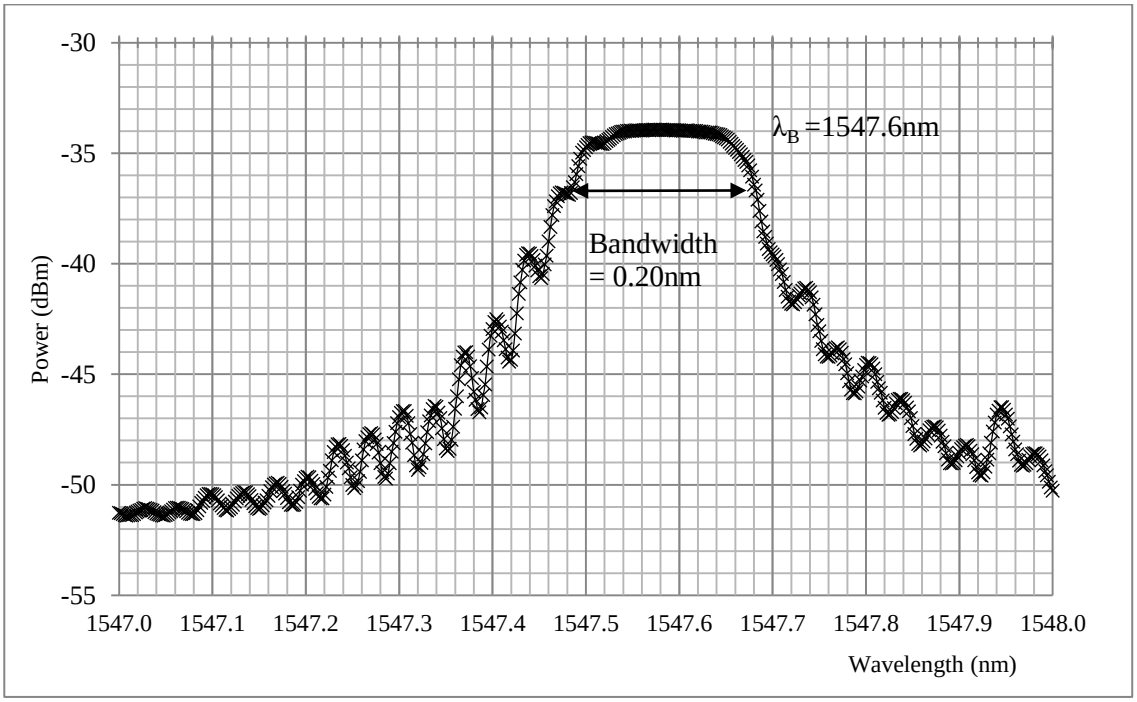

(b)

Figure 4. 2: Reflection spectrum of FBGs fabricated.

4.2 Construction of Distributed Bragg Reflector Fibre Laser

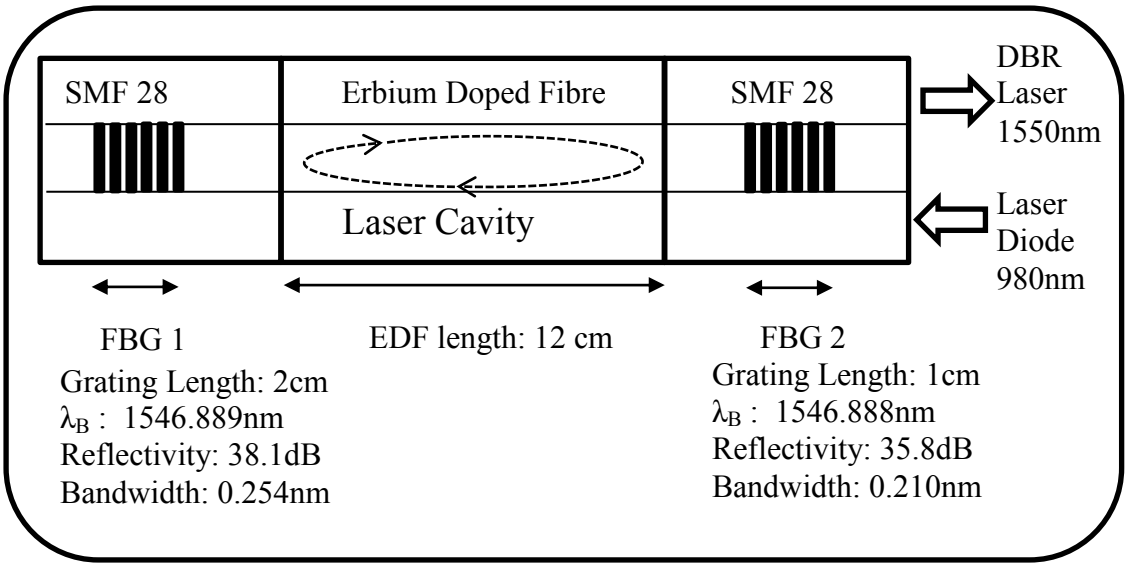

Figure 4. 3: Schematic of constructed DBR.

In this experiment, DBR was constructed from FBGs with slightly different grating lengths and that they have different reflectivity but negligible difference in Bragg wavelengths and a segment of Erbium-doped fibre (EDF) as shown in Figure 4.3. The bandwidth of the FBGs and the cavity length are the main properties to determine the number of longitudinal modes within the resonator and output laser stability.

Matching Bragg wavelengths FBGs are crucial so that both FBGs only reflect the same wavelengths within the cavity and transmit the others out of the cavity. Therefore, only signals with the Bragg wavelengths will oscillate within the gratings and get amplified.

Difference in lengths of the gratings between FBG1 (2cm) and FBG1 (1cm) leads to higher reflectivity in FBG1 (38.1dB) and lower reflectivity in FBG2 (35.8dB) as shown in the simulations in Section 4.1. It is important to have the FBGs

with sufficiently high reflectivity as mirrors shorten the cavity and prevent loss of signal while oscillating within the cavity. FBG 1 which has the higher reflectivity (38.1dB) will reflect more signal power with Bragg wavelengths back into the cavity. On the other hand, FBG2 which has the lower reflectivity (35.8dB) will allow higher output laser emission through it after the signal is being amplified within the cavity. On top of that, FBG 2 having smaller bandwidth is more sensitive to changes. Therefore, larger laser output emission can be obtained with a longer gain medium.

4.3 Experiment

4.3.1 Response of DBR towards pump powers

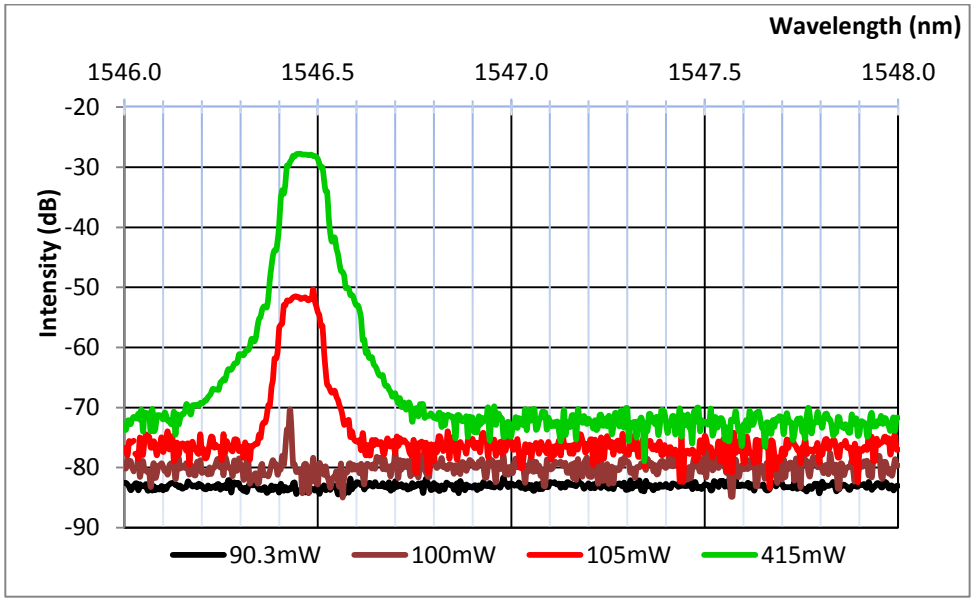

Figure 4. 4: Reflection spectrum of DBR laser with different pump power.

Figure 4.4 presents the reflection spectrum of DBR laser with different pump power. A narrower bandwidth of DBR laser which is approximately 0.11nm is observed compared to the bandwidth of standalone FBG. This may be due to the wavelength of the excited laser is most probably located at the peak wavelength of the reflection curve of the FBG. More pumping energy will go to the excited laser wavelength and the laser power will increase. The linewidth of the laser will be smaller than the bandwidth of the FBG.

On top of that, reflectivity of DBR increases with higher pump power. The laser performance of the DBR with different pump power is illustrated in Figure 4.5. As presented, higher pump power will give higher output power from DBR. These outstanding performances of DBR makes it a suitable device to be used in applications for longer sensing distance.

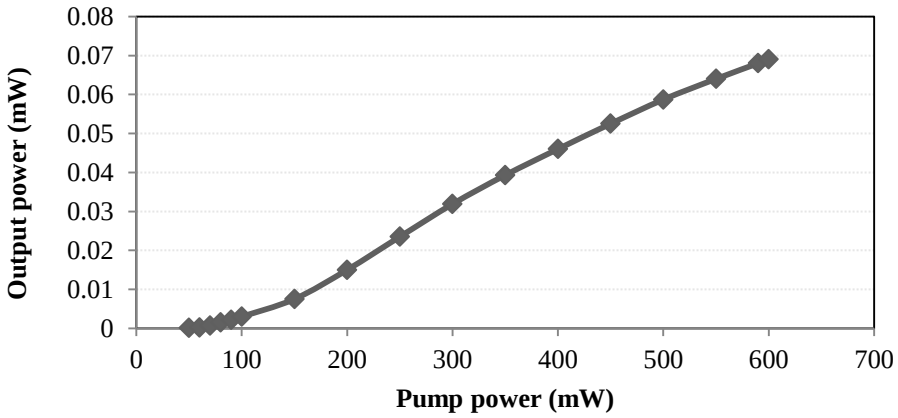

Figure 4. 5: The output performance of the DBR with increasing pump power.

4.3.2 DBR response on acoustic pressure

Experiment was done according to the experimental setup shown in Figure 3.3. Since neither isolator nor circulator was used in the setup, the free end of DBR was dipped into an index matching gel (as shown in Figure 4.6) to scatter the lights at the fibre end and prevent back reflection of lights into the pump laser.

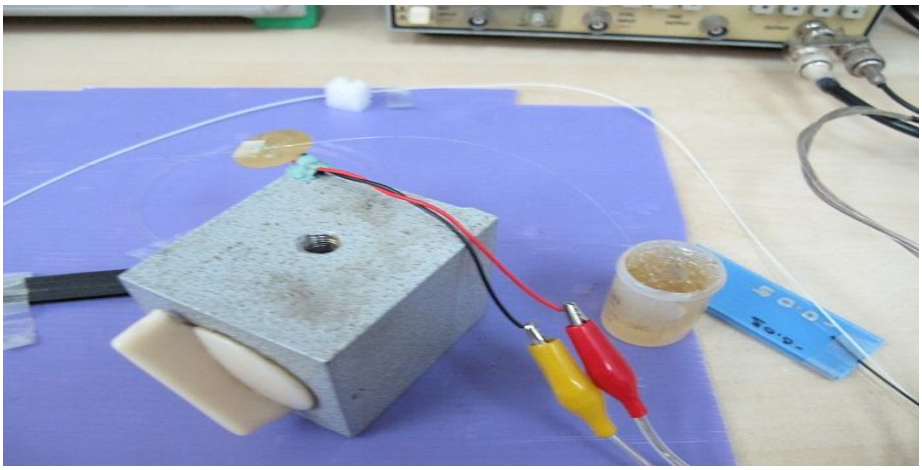

Figure 4. 6: Fibre end of DBR being dipped into index matching gel.

As mentioned in Section 3.2, a piezoelectric transducer (PZT) was used to generate acoustic waves into the system when connected to a function generator. According to the setup in Figure 3.3, PZT is placed nearer to FBG 1. Since the EDF used was 12cm in length, attenuation along the fibre causes the acoustic vibrations from the PZT to have little influence on FBG 2. On top of that, FBG 2 being shorter in terms of grating length has lower sensitivity. Therefore, it is assumed that in this configuration, only FBG 1 was subjected to the influence of acoustic wave and the DBR output response is similar to the FBG.

As a start for this section of experiment, the frequency of the background was first obtained by conducting the experiment without introducing any vibrations from PZT and the output signal from DBR is recorded using the oscilloscope. Data from the

oscilloscope are in time base Figure 4.7, so fast fourier transformation using Matlab codes was performed to analyse the data as attached in Appendix 2.

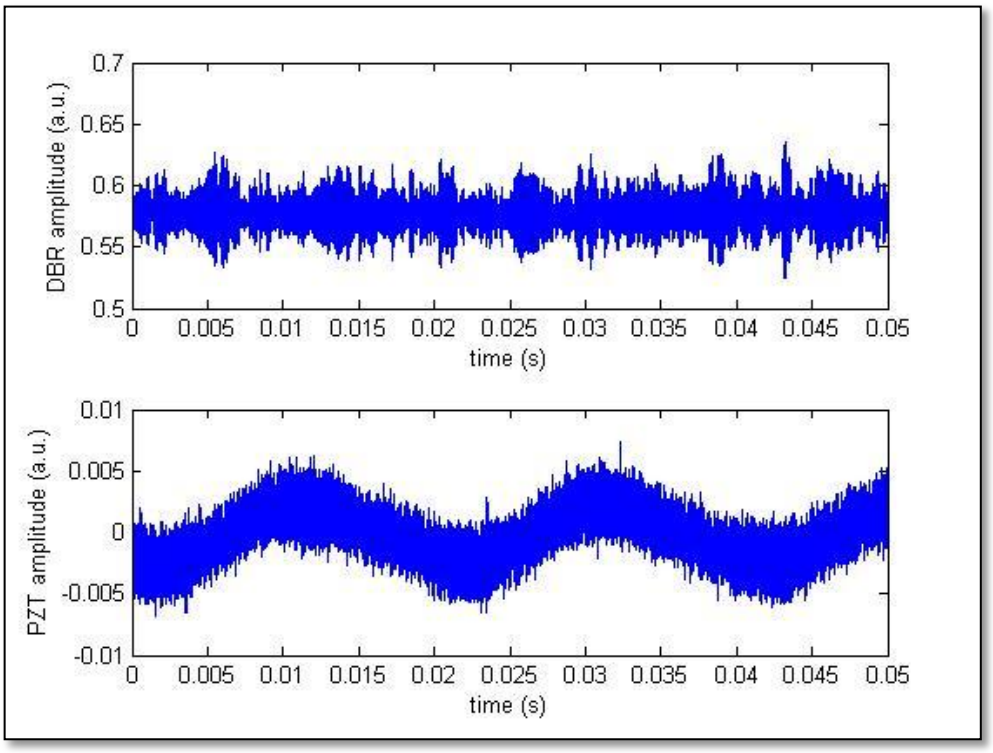

Figure 4. 7: Amplitude of background noise

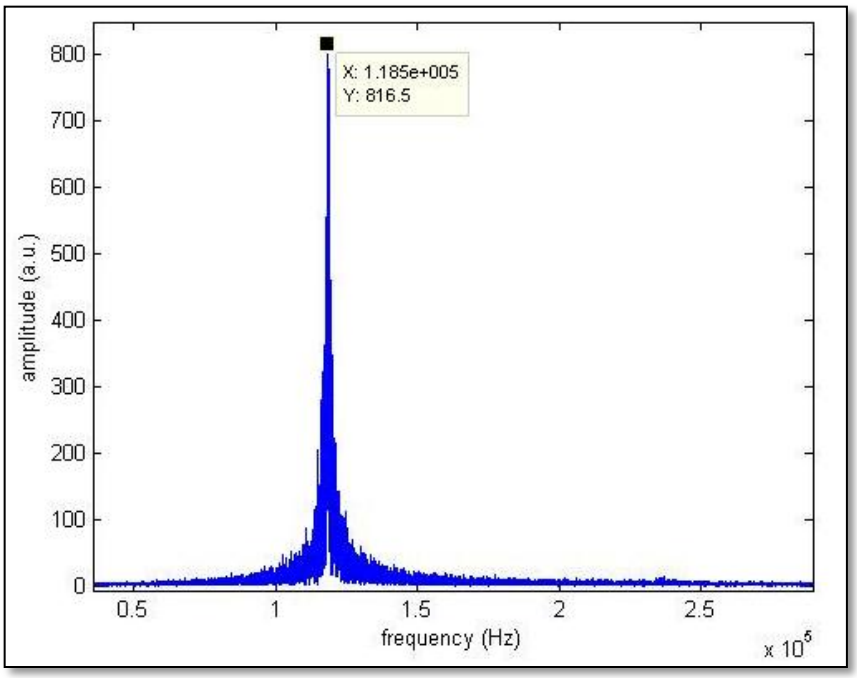

Figure 4. 8: Frequency of background noise

As shown in Figure 4.8, the frequency of background noise is approximately 110 kHz. Hence, selection of frequency for the experiment was above this frequency i.e. 120 kHz and onwards.

Figure 4.9 presents the experimental results of the DBR acousto-optically modulated at 150 kHz which is within the vicinity of the resonant frequency of the PZT. The experiment is then further explored with a lower frequency of 140 kHz and a higher frequency of 160 kHz. The results from the exploration are as shown in Figure 4.10 and Figure 4.11 respectively. It is observed that the acoustic vibration causes distortion in output signals of DBR. Furthermore, the distortion of signal is found to increase with the growing of impinging acoustic pressure which was done by increasing the amplitude of the signal as portrayed in Figure 4.12.

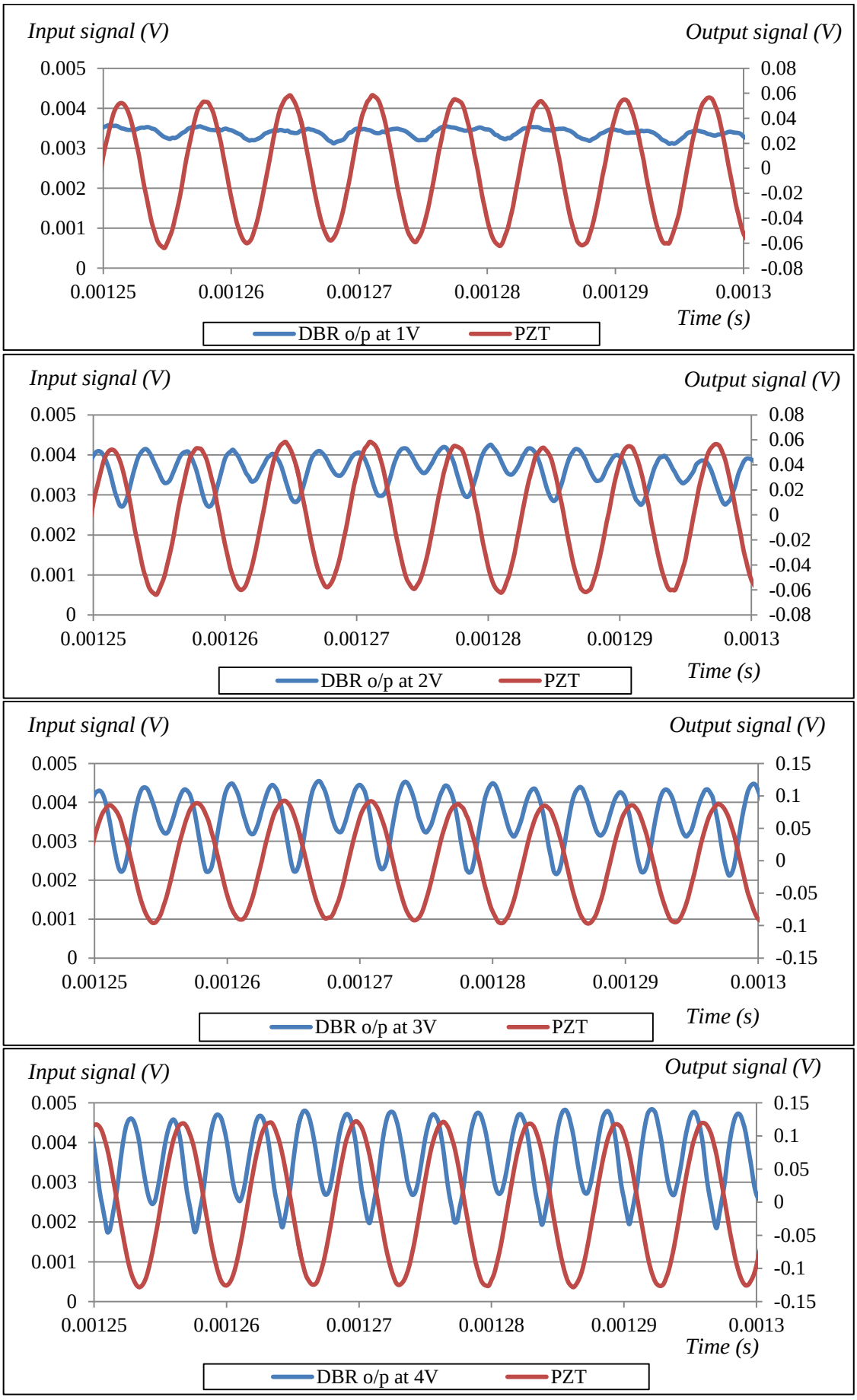

Figure 4. 9: Experimental results of the DBR acousto-optically modulated at 150 kHz.

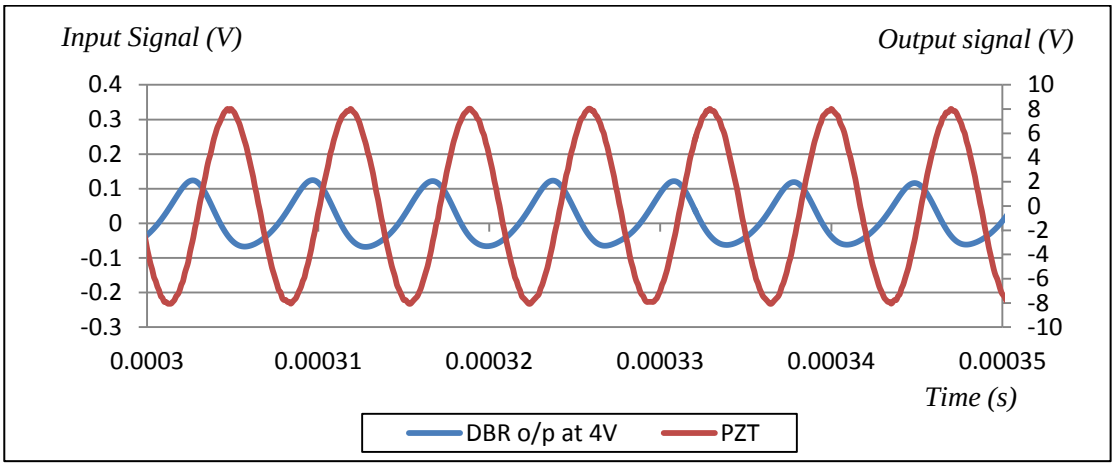

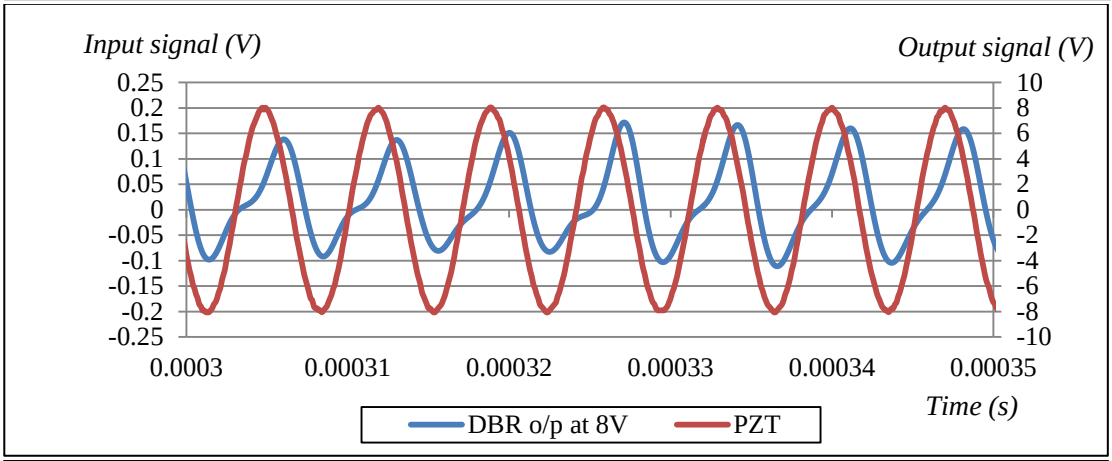

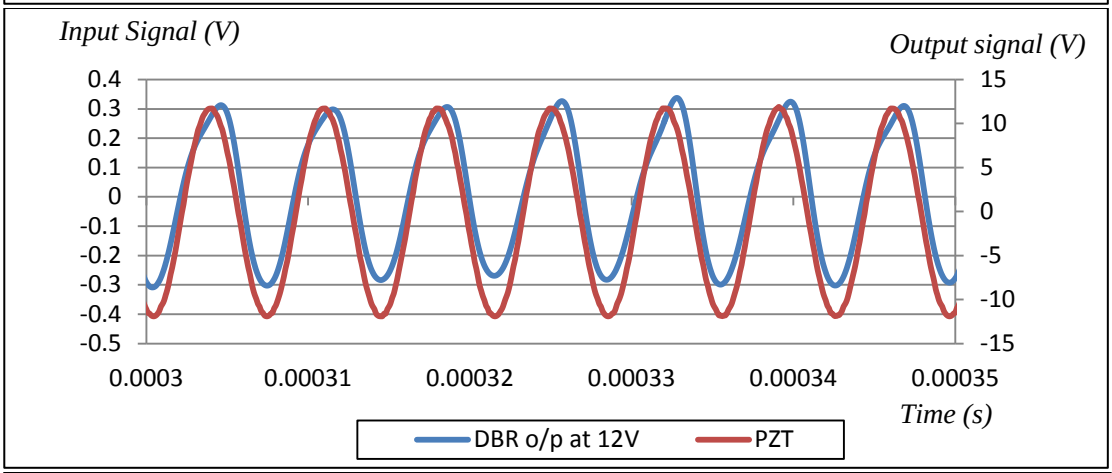

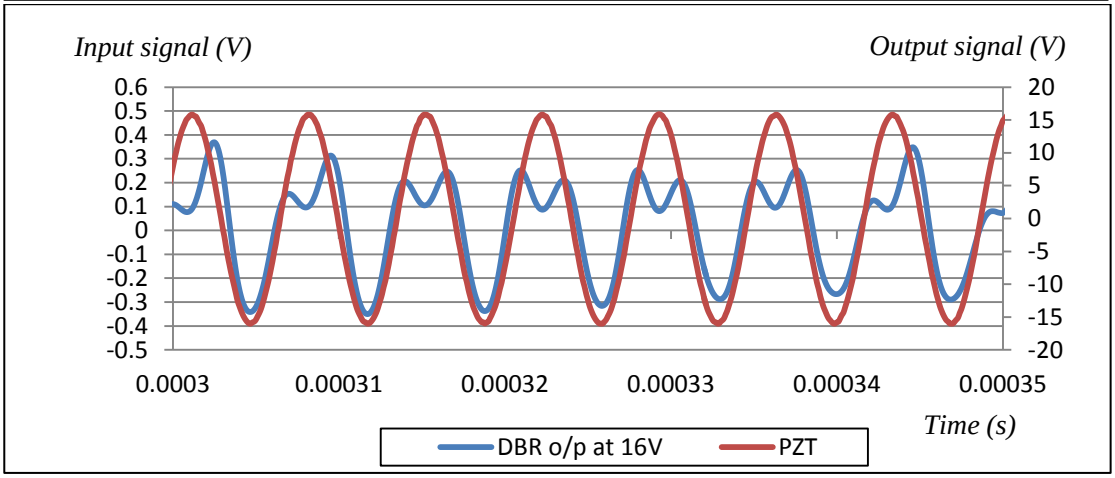

Figure 4.10: Experimental results of the DBR acousto-optically modulated at 140 kHz.

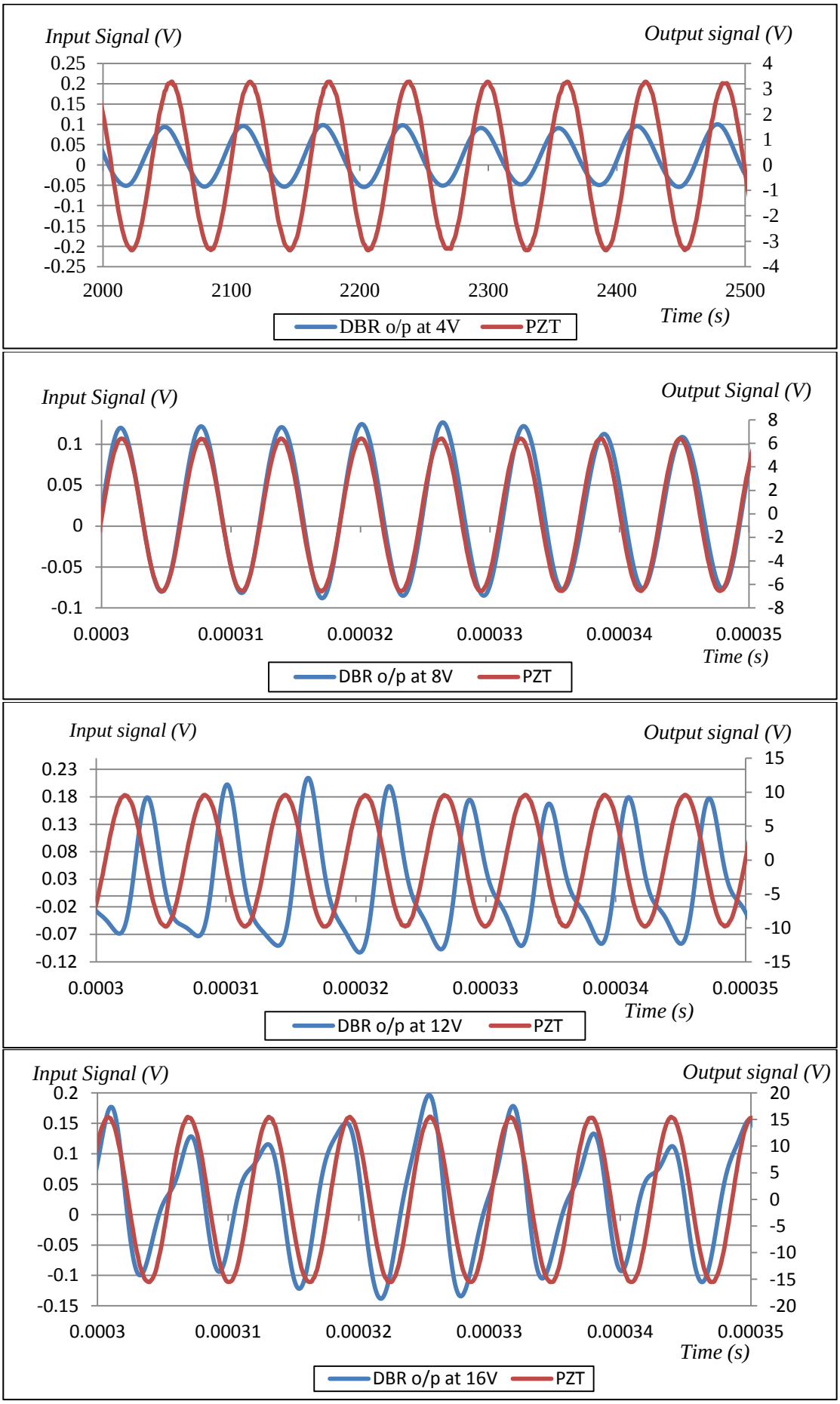

Figure 4.11: Experimental results of the DBR acousto-optically modulated at 160 kHz.

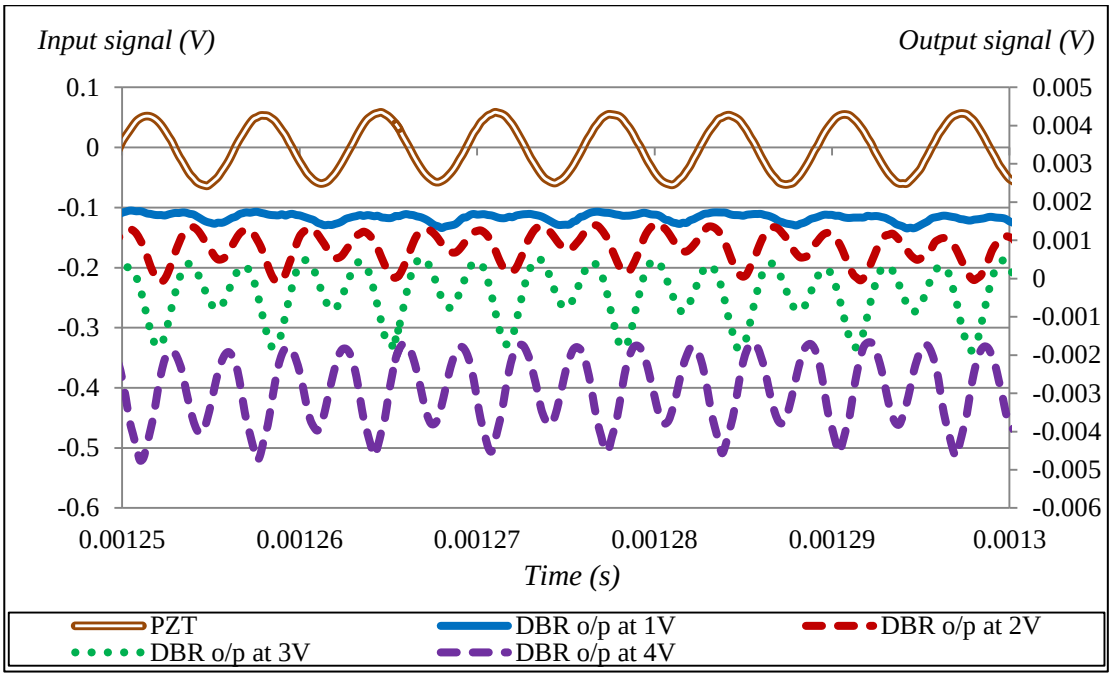

(a) Frequency of PZT: 150 kHz

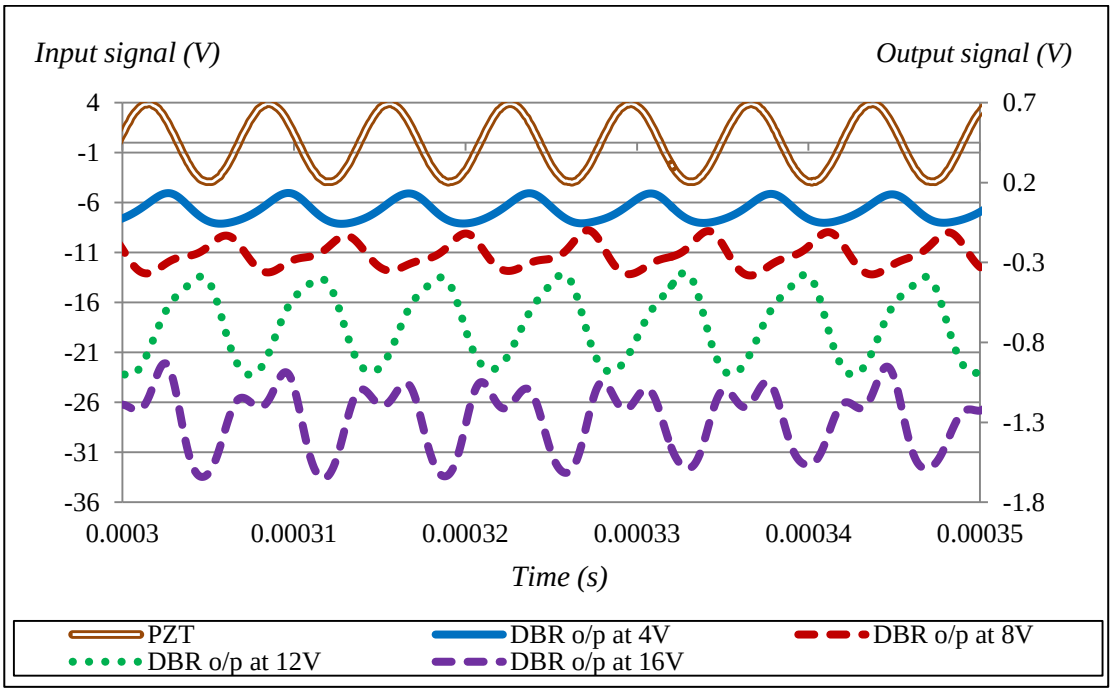

(b)Frequency of PZT: 140 kHz

Figure 4.12: Experiment results showing increase in distortion with increasing acoustic pressure for different frequencies of PZT(a) 150 kHz , (b) 140 kHz and (c) 160 kHz

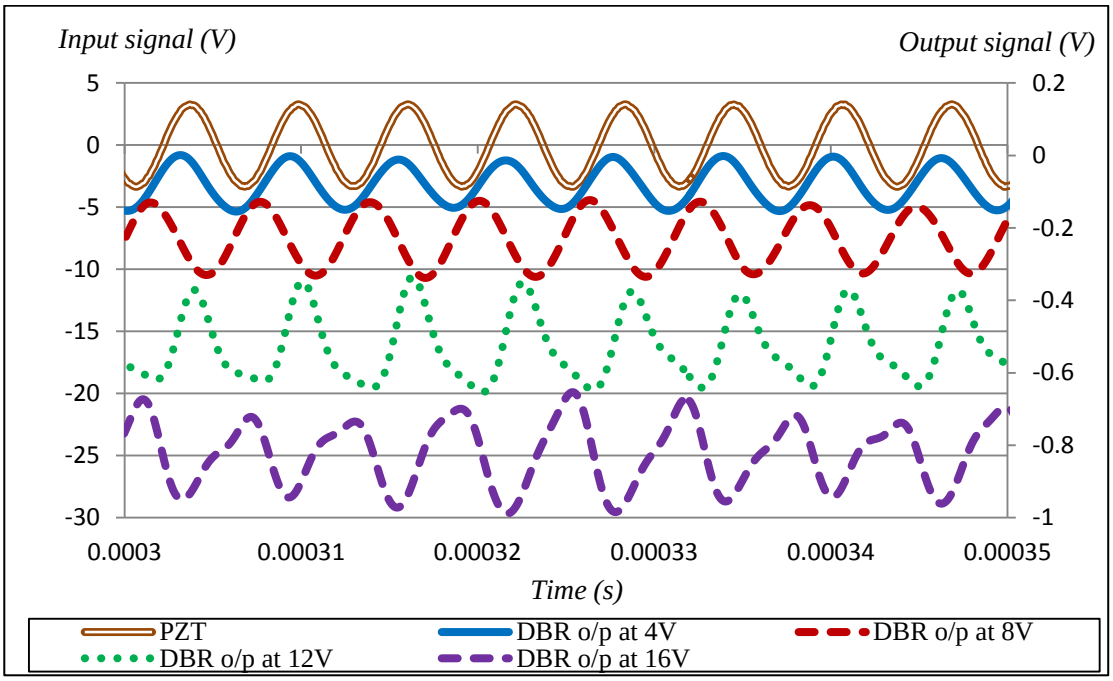

(c) Frequency of PZT: 160 kHz

Figure 4.12, continued: Experiment results showing increase in distortion with increasing acoustic pressure for different frequencies of PZT (a) 150 kHz , (b) 140 kHz and (c) 160 kHz

To validate the experimental results, a theoretical analysis was carried out to evaluate the output response of the DBR that was acoustically modulated by PZT using Matlab codes as attached in Appendix 3. Figure 4.13 presents the simulation and the experimental results of the DBR acousto-optically modulated at 150 kHz. It is confirmed that the simulations and experimental results are similar whereby both shows distortion in the output response of DBR and the distortion increases with the increase of impinging acoustic pressure.

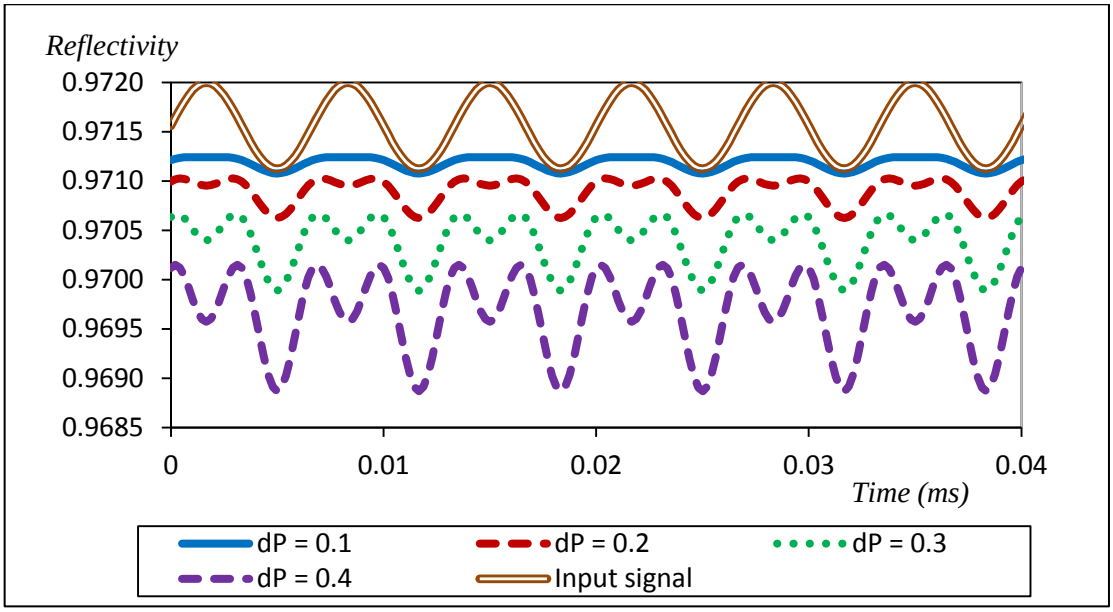

(a)Simulation

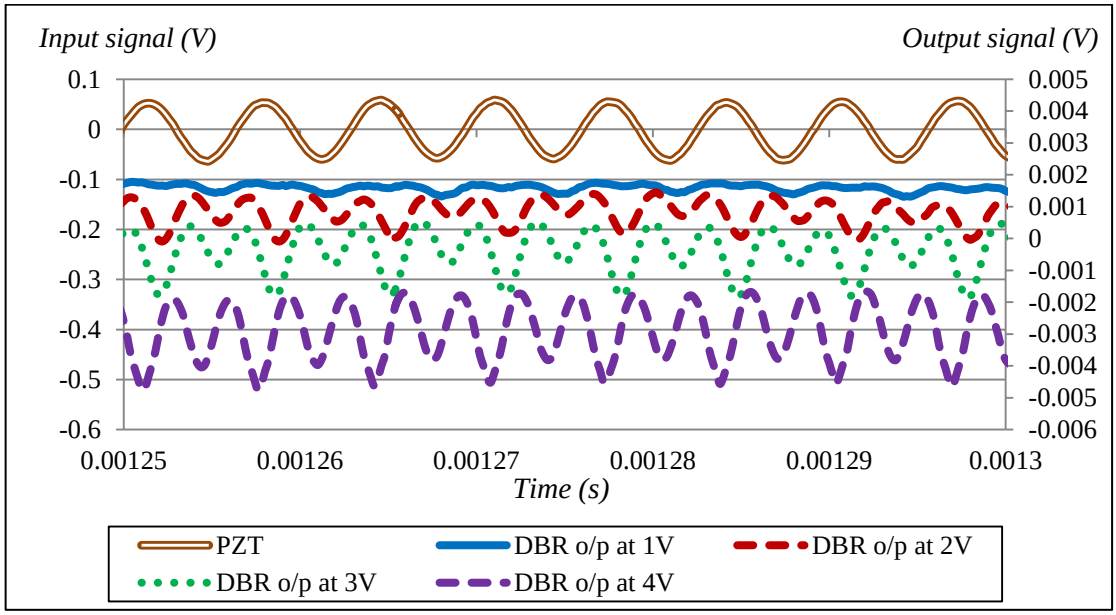

(b) Experiment

Figure 4. 13: Comparison between the (a) simulation and (b) experiment results.

4.3.3 Frequency response of DBR

The magnitude of distortion can be interpreted from the amplitude of the second harmonics as illustrated in Figure 4.14(a). Here, it is shown that the harmonic has a frequency which is two times as much as the incident acoustic wave frequency. On top of that, the generated second harmonic amplitude is higher and may supersede the amplitude of the fundamental frequency when the amplitude of input is high.

Figure 4.14(b) illustrate similar frequency responses but with different magnitudes of distortion due to the frequency dependent vibration strength of the PZT.

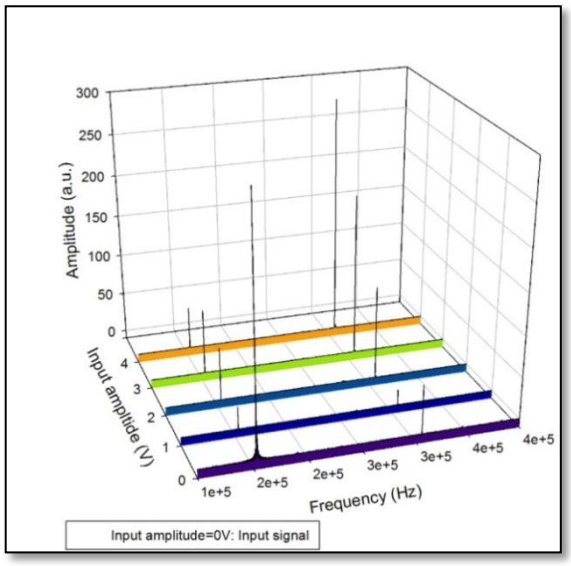

(a)

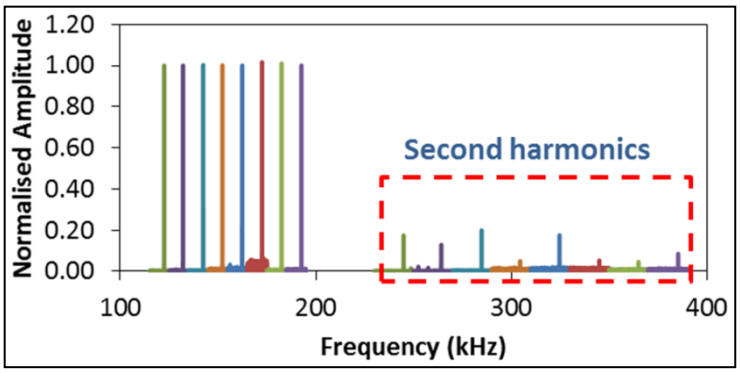

(b)

Figure 4. 14: Output frequency responses of the DBR for different (a) input amplitude and (b) frequency

Chapter 5

Conclusion and Future Work

5.1 Conclusion

All the objectives of the project have been achieved by the end of this project. Many types of FBG vibration sensing system, like linear FBG sensing system, ring laser FBG sensing system and finally DBR structured FBG sensing system have been explored. Due to lack of data obtained from the other systems, only DBR structured sensor response to acoustic wave is presented in this project.

Length of gain medium and reflectivity of FBGs are the determining factor of a good DBR. Shorter length of gain medium like rare-earth fibre will have higher chances of providing single longitudinal mode resonation within the cavity for better stability of laser but will give a lower throughput power. Higher reflectivity in FBGs creates a better reflection mirror hence preventing energy loss when oscillating within resonator. In this project, DBR is designed to have one FBG having lower reflective bandwidth than the other and the results show that there are significant improvements in throughput power although paired with a longer length of gain medium.

In terms of acoustic sensing system, DBR under the influence of acoustic waves shows significant distortion in the output signal. When compared with the theoretical simulation, experimental results show great match to the simulations. Also in this project, distorted output signal is found to be able to create second harmonic components and the amplitude of the second harmonic depends on the strength of the acoustic waves. This acousto-optic behaviour of DBR is an important discovery for better design of optical vibration sensor system in the future.

5.2 Future work

Since there is still a lot of room for improvement in this project, the proposed future works are:

1. To fabricate shorter Bragg grating.
2. To construct DBR by direct photowriting two matching Bragg wavelength on active material using higher energy laser source like 193nm excimer laser to provide lower threshold so that inter-cavity splice loss can be eliminated.
3. To use shorter EDF in DBR fabrication to ensure better stability in DBR laser.

References

A. Othonos, K. Kyriacos, D. Pureur and A. Mugnier, 2006, "*Wavelength Filters in Fibre Optics*", Springer Series in Optical Sciences Vol. **123**, 189-269.

B. Malo, K. O. Hill, F. Bilodeau, D. C. Johnson, and J. Albert, 1993, "Point-by-point fabrication of micro-Bragg gratings in photosensitive fibre using single excimer pulse refractive index modification techniques," Electron. Lett. **29**.

Bahaa E.A. Saleh , Malvin Carl Teich, 1991, " *Fundamentals of Photonics"*, John Wiley & Sons, Inc, 1991.

Bai-Ou Guan, Hwa-Yam Tam, Sien-Ting Lau and Helen L.W.Chan, 2005, "*Ultrasonic Hydrophone Based on Distributed Bragg Reflector Fibre Laser"*, IEEE Photonics Technology Letters, Vol.**16**.

C.C. Ye and R.P. Tatam, 2005, "*Ultrasonic sensing using Yb^{3+}/Er^{3+}-codoped distributed feedback fibre grating lasers",* Smart Materials and Structures.

Chengang Lyu, Chuang Wu, Hwa-Yam Tam, Chao Lu and Jianguo Ma, 2013, *"Polarimetric heterodyning fibre laser sensor for directional acoustic signal measurement"*, Optics Express.

D.C. Seo, D.J. Yoon, I.B. Kwon and S.S. Lee, 2009, *"Sensitivity enhancement of fibre optic FBG sensor for acoustic emission",* SPIE Vol. **7294**.

Francis T.S. Yu, Shizhuo Yin, 2002, "*Fibre Optic Sensors (Optical Science and Engineering)*", CRC Press.

G.B.Hocker, 1979, *"Fibre-optic sensing of pressure and temperature"*, Applied Optics, Vol. **18**, pp. 1445-1448.

Guan B.O, Jin L. , Zhang Y. and Tam H.Y., 2012, "*Polarimetric Heterodyning Fibre Grating Laser Sensors",* Journal of Lightwave Technology, Vol. **30**.

Hiroshi Tsuda, 2010, "*Fibre Bragg grating vibration-sensing system, insensitive to Bragg wavelength and employing fibre ring laser"*, Optics Letters, Vol. **35**.

Hiroshi Tsuda, 2011,"*A Bragg Wavelength-Insensitive Fibre Bragg Grating Ultrasound Sensing System that Uses a Broadband Light and No Optical Fibre",* Journal of Sensors.

Kenneth O. Hill and Gerald Meltz, 1997,"*Fibre Bragg Grating Technology Fundamentals and Overview"*, Journal of Lightwave Technology, Vol.**15.**

M.I. Comanici, Lv Zhang, Lawrence R.Chen, Xijia Gu, Lutang Wang and Peter Kung, 2012, *"All Fibre DBR-Based Sensor Interrogation System for Measuring Acoustic Waves",* Journal of Sensors, 862078.

Pavel Fomitchov and Sridhar Krishnaswamy, 2003,"*Response of a fibre Bragg grating ultrasonic sensor"*, Optical Engineering, Vol. **42**.

Raman Kashyap, 1999, "*Fibre Bragg Gratings"*, Academic Press, United States of America.

Rao Y.J, 1997,"*In-fibre Bragg grating sensors"*,Measurement science and technology, Vol. **8**, pp. 355-375.

S.O.Kasap, 2001, "*Optoelectronics and Photonics: Principles and Practices"*, Prentice Hall, New Jersey.

T. Erdogan , 1997, "*Fibre Grating Spectra",* Journal of Lightwave Technology, Vol.**15**, pp1277-1294.

Yang Zhang and Bai-Ou Guan, 2009, "*High-Sensitivity Distributed Bragg Reflector Fibre Laser Displacement Sensor",*IEEE Photonics Technology Letters, Vol. **21**.

Yang Zhang, Bai-Ou Guan and Hwa-Yam Tam, 2008,*"Characteristics of the distributed Bragg reflector fibre laser sensor for lateral force measurement"*, Journal of Optics Communications.

Zhang, Y., Guan B.O.Guan and Tam H.Y, 2009, "*Ultra-short distributed Bragg reflector fibre laser for sensing applications"*, Optics Express, Vol. **17**.

Zhi Zhou, Thomas W. Graver, Luke Hsu, Jin-Ping Ou, 2003, "*Techniques of Advanced FBG sensors: fabrication, demodulation, encapsulation and their application in the structural health monitoring of bridges*", Pacific Science Review, Vol. **5**.

Appendix 1: Matlab codes for simulation of effect of grating lengths

```
clear all
clc;
nef = 1.445;          %effective index
dn = 0.2E-04;           %index modulation
lg = 1558E-09;         %reflection wavelength
period = lg/(2*nef);
tic
N_lamb = 1001; % no. of sample for lambda
L = 0.02;
lamb = linspace(1557.5E-9,1558.5E-09,N_lamb); % wavelength lambda
disp = linspace(0,L,200);  %displacement
dz = disp(2)-disp(1);
FWHM = 0.01;
m = 1;
alpha = 4;
for l=lamb;
    F = [1 0; 0 1];
    dn_z = dn; %uniform
    del = 2*pi*nef*(1/l - 1./lg);
    sig = 2*pi*dn_z./l;
    g = sig + del;

    k = pi*dn_z/l;
    p1 = sqrt(k^2 - g^2);

    r_an(m) = k*sinh(p1*L);
    r_an(m) = r_an(m)./(i*p1*cosh(p1*L)+g*sinh(p1*L));
    t_an(m) = p1./(i*p1*cosh(p1*L)+g*sinh(p1*L));
    g2 = -alpha + i*(sig + del);
    p2 = sqrt(g2^2+k^2);
    r_an_loss(m) = -i*k*sinh(p2*L);
    r_an_loss(m) = r_an_loss(m)./(p2*cosh(p2*L)-g2*sinh(p2*L));
    t_an_loss(m) = p2./(p2*cosh(p2*L)-g2*sinh(p2*L));

    T_an(m) = abs(t_an(m)).^2;
    T_an_loss(m) = abs(t_an_loss(m)).^2;
    R_an(m) = abs(r_an(m)).^2;
    R_an_loss(m) = abs(r_an_loss(m)).^2;
    for z = disp
        A = cosh(p1*dz);
        B = i*(g/p1)*sinh(p1*dz);
        f11 = A - B;
        f12 = -i*(k/p1)*sinh(p1*dz);
        f21 = -f12;
        f22 = A + B;
        ff  = [f11 f12; f21 f22];
        F = ff*F;
        loss = [exp(10*dz) 0 ; 0 exp(-10*dz)];
```

```
        F1 = loss*F;
    end

    r_nu(m) = F(2,1)/F(1,1);
    R_nu(m) = (abs(r_nu(m)))^2;
    t_nu(m) = 1/F(1,1);
    T_nu(m) = (abs(t_nu(m)))^2;
    r_nu_loss(m) = F1(2,1)/F1(1,1);
    t_nu_loss(m) = exp(-alpha*L)/F1(1,1);
    R_nu_loss(m) = (abs(r_nu_loss(m)))^2;
    T_nu_loss(m) = (abs(t_nu_loss(m)))^2;
    m=m+1;
end

toc
figure(1)

subplot(211)
plot(lamb*1e9,10*log10(R_nu),'k',lamb*1e9,10*log10(R_nu_loss),'b')
title('Comparison between lossy and lossless FBG - Numerical');
subplot(212)
plot(lamb*1e9,10*log10(T_nu),'k',lamb*1e9,10*log10(T_nu_loss),'b')
legend('lossless','lossy')

figure(2)
subplot(411)
plot(lamb*1e9,10*log10(R_an),'k',lamb*1e9,10*log10(R_an_loss),'b')
title('Comparison between lossy and lossless FBG - Analytical');
subplot(412)
plot(lamb*1e9,10*log10(T_an),'k',lamb*1e9,10*log10(T_an_loss),'b')
legend('lossless','lossy')
subplot(413)
plot(lamb*1e9,10*log10(T_an),'k',lamb*1e9,10*log10(T_nu),'b--')
legend('Analytical','Numerical')
subplot(414)
plot(lamb*1e9,10*log10(T_an_loss),'k',lamb*1e9,10*log10(T_nu_loss),'b--')
legend('Analytical','Numerical')

data =[lamb'*1e9 R_nu'];
```

Appendix 2: Matlab codes for transformation from time-based to frequency-based.

```
clear all;
clc;
file_no = 1078:1078;
data=[];
data_f=[];
data2=[];
data2_f=[];
for x = file_no
    fn = ['LIM-' num2str(x) '.CSV'];
    M = xlsread(fn,'A21:A500021');
    M2= xlsread(fn,'B21:B500021');
    dt = xlsread(fn,'B6:B6');
    t = 0:dt:500000*dt;
    fs = 1/dt;
    figure(1)
     subplot(211)
     plot(t', M)
     xlabel ('time (s)')
     ylabel ('DBR amplitude (a.u.)')
     subplot(212)
     plot (t', M2)
     xlabel ('time (s)')
     ylabel ('PZT amplitude (a.u.)')
     f = linspace(0, fs/2, (size(t,2)+1)/2);
     M_f = abs(fftshift(fft(M-mean(M))));
     M_f = M_f(((size(t,2)+1)/2):end);
    clear M_f;

    f = linspace(0, fs/2, (size(t,2)+1)/2);
    M_f = fft(M-mean(M));
    M_ff = abs(fftshift(M_f));
    M_ff = M_ff(((size(t,2)+1)/2):end);
    M2_f = fft(M2-mean(M2));
    M2_ff = abs(fftshift(M2_f));
    M2_ff = M2_ff(((size(t,2)+1)/2):end);
    f = linspace(0, fs/2, (size(t,2)+1)/2);
    M_f = abs(fftshift(fft(M-mean(M))));
    M_f = M_f(((size(t,2)+1)/2):end);
    M2_f = abs(fftshift(fft(M2-mean(M2))));
    M2_f = M2_f(((size(t,2)+1)/2):end);
    data = [data M];
    data_f = [data_f M_f];
    data2 = [data2 M2];
    data2_f = [data2_f M2_f];
    figure(2)
    subplot(111)
    plot(f', M_f, 'k',f', M2_f, 'b')
    plot(f', M_f)
    xlabel ('frequency (Hz)')
    ylabel ('amplitude (a.u.)')

end
```

```
data = [t' data];
data_f = [f' data_f];
data2 = [t' data2];
data2_f = [f' data2_f];

csvwrite('data.txt',data);
csvwrite('data_f.txt',data_f);
```